

1 Simulating the effect of subsurface drainage on the thermal regime 2 and ground ice in blocky terrain, Norway

3 Cas Renette^{1,2}, Kristoffer Aalstad¹, Juditha Aga¹, Robin Benjamin Zweigel^{1,2,3}, Bernd Etzelmüller¹,
4 Karianne Staalesen Lilleøren¹, Ketil ~~Isaksen~~³Isaksen⁴, Sebastian Westermann¹

5
6 ¹Department of Geosciences, University of Oslo, Oslo, Norway

7 ~~²Centre~~²Department of Earth Sciences, University of Gothenburg, Gothenburg, Sweden

8 ³Centre for Biogeochemistry of the Anthropocene, UiO, Oslo

9 ~~³Norwegian~~⁴Norwegian Meteorological Institute, Oslo, Norway

10 Correspondence to: Cas Renette (cas.renette@~~gmail.com~~gvc.gu.se)

11 **Abstract.** Ground temperatures in coarse, blocky deposits such as mountain blockfields and rock glaciers have long been
12 observed to be lower in comparison with other (sub)surface material. One of the reasons for this negative temperature anomaly
13 is the lower soil moisture content in blocky terrain, which decreases the duration of the zero curtain in autumn. Here we used
14 the CryoGrid community model to simulate the effect of drainage on the ground thermal regime and ground ice in blocky
15 terrain permafrost at two sites in Norway. The model setup is based on a one-dimensional model domain and features a surface
16 energy balance, heat conduction and advection, as well as a bucket water scheme with adjustable lateral drainage. We used
17 three idealized subsurface stratigraphies, ~~denoted~~blocks only, blocks with sediment and sediment only ~~and are, which can be~~
18 either drained (i.e. with strong lateral subsurface drainage), or undrained of water, (i.e. without drainage), resulting in six
19 ~~scenarios~~scenarios. The main difference between the three stratigraphies is their ability to retain water against drainage: while
20 the *blocks only* stratigraphy can only hold small amounts of water, much more water is retained within the sediment phase of
21 the two other stratigraphies, which critically modifies the freeze-thaw behaviour.

22 The simulation results show markedly lower ground temperatures in the *blocks only, drained* scenario compared to
23 other scenarios, with a negative thermal anomaly of up to 1.8–2.2 °C. For this scenario, the model can in particular simulate
24 the time evolution of ground ice, with build-up during and after snow melt and spring and gradual lowering of the ice table in
25 the course of the summer season. The thermal anomaly increases with larger amounts of snowfall, showing that well drained
26 blocky deposits are less sensitive to insulation by snow than other soils. We simulate stable permafrost conditions at the
27 location of a rock glacier in northern Norway with a mean annual ground surface temperature of 2.0–2.5 °C in the *blocks only,*
28 *drained* simulations. Finally, transient simulations since 1951 at the rock glacier site (starting with permafrost conditions for
29 all stratigraphies) showed a ~~complete or partial~~100% lowering of the ground ice table ~~since 1951 for all simulations except in~~
30 the *blocks* with sediment, drained run, 37% lowering in the sediment only, drained run
31 and only 2% lowering in the blocks only, drained run. The interplay between the subsurface water/ice balance and ground
32 freezing/thawing driven by heat conduction can at least partly explain the occurrence of permafrost in coarse blocky terrain

33 below the ~~assumed~~ elevational limit of permafrost: in non-blocky sediments. It is thus important to consider ~~this effect~~the
34 subsurface water/ice balance in blocky terrain in future efforts on permafrost distribution mapping in mountainous areas.
35 Furthermore, an accurate prediction of the evolution of the ground ice table in a future climate can have implications for slope
36 stability, as well as water resources in arid environments.

37 **1 Introduction**

38 Permafrost is defined as ground that remains at or below 0 °C for two or more consecutive years (Van Everdingen, 1998) ~~and~~.
39 It is a common feature in the Arctic and high mountain environments, where permafrost occurs even in mid- and low latitudes
40 (Gorbunov, 1978). Different permafrost zones are classified based on the aerial extent of permafrost presence. These zones
41 are: continuous, discontinuous, sporadic and isolated, where the surface is underlain by permafrost in more than 90%, 50-
42 90%, 10-50% and less than 10% of the land area, respectively (Smith and Riseborough 2002). Snow is an important factor in
43 governing ground temperatures and permafrost distribution within an area (e.g. Zhang et al., 2001; Zhang 2005; Goodrich,
44 1982), especially in mountain areas where permafrost is often associated with a shallow snow cover (e.g. Gislås et al., 2014;
45 Luetsch et al., 2004). The influence of soil moisture is complicated as it has an impact on the surface energy balance (e.g
46 Liljedahl et al., 2011), the thermal characteristics of the soil (e.g. Göckede et al., 2017), and freezing/thawing dynamics (e.g.
47 Hinkel et al., 2001; Hinkel and Outcalt, 1994), which can lead to both lower and higher ground temperatures. Finally, the
48 properties of the subsurface material can strongly influence permafrost distribution. In discontinuous mountain permafrost
49 terrain, the lowest-lying ~~active~~ permafrost ~~landforms~~areas are frequently found in coarse, blocky terrain (Harris and Pedersen,
50 1998). In particular, rock glaciers are frequently found below the ~~assumed elevational~~general elevation limit of mountain
51 permafrost (Lilleøren and Eitzelmüller 2011).

52 ~~The occurrence of a negative temperature anomaly in coarse, blocky deposits has long been recognized, e.g. in central~~
53 ~~eastern~~In Southern Norway ~~by Liestøl (1966). Harris and Pedersen (1998) found a negative temperature anomaly of 4 to 7 °C~~
54 ~~in blocky terrain relative to adjacent mineral sediment in mountains in Canada and China. They summarized four hypotheses~~
55 ~~that explain these anomalies: (a) The Balch effect; (b) chimney effect; (c) evaporation of water and sublimation of ice in the~~
56 ~~summer and (d) continuous air exchange with the atmosphere when no continuous winter snow cover is present.~~

57 ~~Juliussen and Humlum (2008) showed that block fields in the Norwegian mountains featured a negative temperature~~
58 ~~anomaly of 1.3 to 2.0 °C, which was mainly attributed to rocks protruding into and through the snow cover which leads to a~~
59 ~~higher effective thermal conductivity of the snow cover. Gruber and Hoetzle (2008) presented a simple model for the conductive~~
60 ~~effect of blocks protruding through the snow cover which showed that the mean annual ground temperature is reduced as a~~
61 ~~result of a lower thermal conductivity of a blocky layer.~~

62 ~~Additionally, a lower soil moisture content in permeable blocky debris decreases the duration of the zero curtain in~~
63 ~~autumn since less latent heat is liberated compared to soil with higher soil moisture content (Juliussen and Humlum 2008). In~~
64 ~~spring, the opposite effect is observed when percolating meltwater refreezes at the bottom of the blocky surface layer and~~

65 confines temperatures at the ice interface to 0 °C (e.g. Juliussen and Humlum, 2008; Hanson and Hoelzle, 2004; Humlum,
66 1997).

67 ~~Rock glaciers play an important role in the hydrological cycle, especially in arid regions like the Andes, where in
68 some areas more water is stored in rock glaciers than in glaciers (Jones et al., 2019; Azócar and Brenning, 2010). The open
69 debris structure can act as a trap for snow and a rock glacier can store a significant quantity of ice or liquid water. Rock glaciers
70 studied in Argentina are an important water resource as they release water mainly during periods of drought (Croce and Milana
71 2002). Ground ice melt as a response to climate warming threatens this water source. Additionally, melting of ground ice can
72 lead to slope instability (e.g. Gruber and Haeblerli, 2007; Saemundsson et al. 2018; Nelson et al., 2001) and damage to
73 infrastructure (e.g. Arenson et al., 2009).~~

74 ~~In southern Norway, limit of mountain permafrost underlies large parts of areas above 1500 m.a.s.l.. The permafrost
75 elevation limit decreases from above is estimated between 1600 m. a.s.l. in the west to about 1100/1000 m. a.s.l. in the eastern,
76 more continental areas east (Etzelmüller et al., 2003). In northern Norway, the limit is around -), while a similar west-east
77 decrease from 800–1000 m.a. a.s.l. to ca. 300 m a.s.l. in the west and decreases towards the east. is observed in Northern
78 Norway (Gisnås et al., 2017). A first Norway-wide inventory of Norwegian rock glaciers based on aerial imagery was
79 published in 2011 (Lilleøren and Etzelmüller, 2011), suggesting that found active permafrost landforms occur above 400
80 m.a.s.l.). The density of rock glaciers in Norway is lower than in other mountain permafrost areas which was attributed to a
81 lack of bedrock competence and debris availability as well as to the relative lack of steep topography above the permafrost
82 limit. Recently, While this first inventory suggested that active rock glaciers occur only above 400 m a.s.l., Lilleøren et al.
83 (2022) recently described rock glaciers near sea level in the area of Hopsfjorden, northern Norway, which feature a limited ice
84 body and are in transition from active to relict. Additionally/ Furthermore, Nesje et al. (2022/2021) presented new evidence for
85 active rock glaciers in southern Norway well below the assumed permafrost limit. Warming of Norwegian mountain
86 permafrost (Etzelmüller limits established in modelling studies (Westermann et al., 2020) is expected to continue in the 21st
87 century (Hipp 2013; Gisnås et al., 2012), resulting in further degradation of these ice bodies and an upward shift of the lower
88 permafrost limit. Hipp et al. (2012) also mentioned the need to address the effect of snow cover and surface material on how
89 ground temperatures respond to climate forcing, 2017).~~

90 ~~Land surface models that can represent permafrost are vital tools to investigate the sensitivity to climate change and
91 complex environmental conditions. Since permafrost presence is often not visible at the surface, numerical modelling based
92 on process understanding is often used to estimate the permafrost distribution (Harris et al. 2009). Rock glaciers play an
93 important role in the hydrological cycle, especially in arid regions like the Andes, where in some areas more water is stored in
94 rock glaciers than in glaciers (Jones et al., 2019; Azócar and Brenning, 2010). The open debris structure can act as a trap for
95 snow and rock glaciers can store significant quantities of ice or liquid water. Rock glaciers studied in Argentina are an
96 important water resource as they release water mainly during periods of drought (Croce and Milana 2002). Sustained ground
97 ice melt as a response to climate warming threatens this water source. Additionally, melting of ground ice can lead to slope~~

98 instability (e.g. Gruber and Haeberli, 2007; Saemundsson et al. 2018; Nelson et al., 2001) and damage to infrastructure (e.g.
99 Arenson et al., 2009).

100 The occurrence of a negative temperature anomaly in coarse, blocky deposits has long been recognized (e.g. Liestøl,
101 1966). Harris and Pedersen (1998) found a negative temperature anomaly of 4 to 7 °C in blocky terrain relative to adjacent
102 mineral sediment in mountains in Canada and China. They summarized four hypotheses that explain these anomalies: (a) The
103 Balch effect; (b) chimney effect; (c) continuous air exchange with the atmosphere when no continuous winter snow cover is
104 present; and (d) evaporation of water and sublimation of ice in the summer. The first three of these driving mechanisms relate
105 to air movement in the blocks, while the last hypothesis links characteristics of the water/ice balance to lower ground
106 temperatures in blocky terrain. In the Norwegian mountains, Juliussen and Humlum (2008) showed that blockfields featured
107 a negative temperature anomaly of 1.3 to 2.0 °C. They state that convection in the blockfields is of low importance in creating
108 the anomaly, while the effect was mainly attributed to rocks protruding into and through the snow cover which leads to an
109 increased heat transfer through the snow cover. Gruber and Hoetzle (2008) presented a simple model for the conductive effect
110 of blocks protruding through the snow cover and showed that the mean annual ground temperature is reduced as a result of a
111 lower thermal conductivity of a blocky layer. Additionally, Juliussen and Humlum (2008) argued that a low soil moisture
112 content in permeable blocky debris (due to subsurface drainage in permeable blocky debris) accelerates active layer refreezing
113 in autumn since less latent heat is liberated compared to soils with higher soil moisture content. Cold winter temperatures can
114 therefore penetrate to deeper layers already in early fall/winter, which may lead to decreased overall winter temperatures.
115 However, in spring, the opposite effect is observed when percolating meltwater refreezes at the bottom of the blocky surface
116 layer, leading to rapid ground warming to 0 °C even in deeper layers (e.g. Juliussen and Humlum, 2008; Hanson and Hoelzle,
117 2004; Humlum, 1997).

118 While many of the mechanisms and processes governing the ground thermal regime of blocky terrain are known, a
119 comprehensive quantitative understanding is still lacking. This is particularly relevant for conceptualization in numerical
120 models which generally do not account for the thermal anomaly of blocky terrain. One-dimensional heat flow models have
121 been used in studies to investigate the effect of climate change on permafrost (e.g. Etzelmüller et al., 2011; Hipp et al., 2012)
122 or to model specific processes in mountain permafrost (e.g. Gruber and Hoetzle, 2008). Since permafrost presence is generally
123 not visible at the surface, numerical models are often used to estimate the permafrost distribution (Harris et al. 2009). However,
124 many such as most models ~~do not~~ neither include a transient representation of the subsurface water and ground ice balance (e.g.
125 Etzelmüller et al., 2011; Hipp et al., 2012; Westermann et al., 2013)-) nor reproduce the thermal anomaly in blockfields (e.g.
126 Obu et al., 2019), the resulting permafrost maps likely show biased ground temperatures and permafrost extent in mountain
127 areas.

128 The CryoGrid community model (Westermann et al., 2022) is a simulation toolbox that can calculate ground
129 temperatures and ~~volumetric water as well as~~ ice content/contents in permafrost environments. It largely builds on the well-
130 established CryoGrid 3 model (e.g. Westermann et al., 2016)-) which has been used in e.g. peat plateaus and palsas (Martin et
131 al., 2021), ice-wedge polygons (Nitzbon et al. 2019) and ~~accommodates~~ boreal forests (Stuenzi et al. 2021) and has a broad

132 range of applications-, including the representation of lateral drainage regimes (Martin et al., 2019), representation of steep
133 rock walls (Schmidt et al., 2021) and massive ice bodies. In the following, the CryoGrid community model is referred to as
134 “CryoGrid” for simplicity.

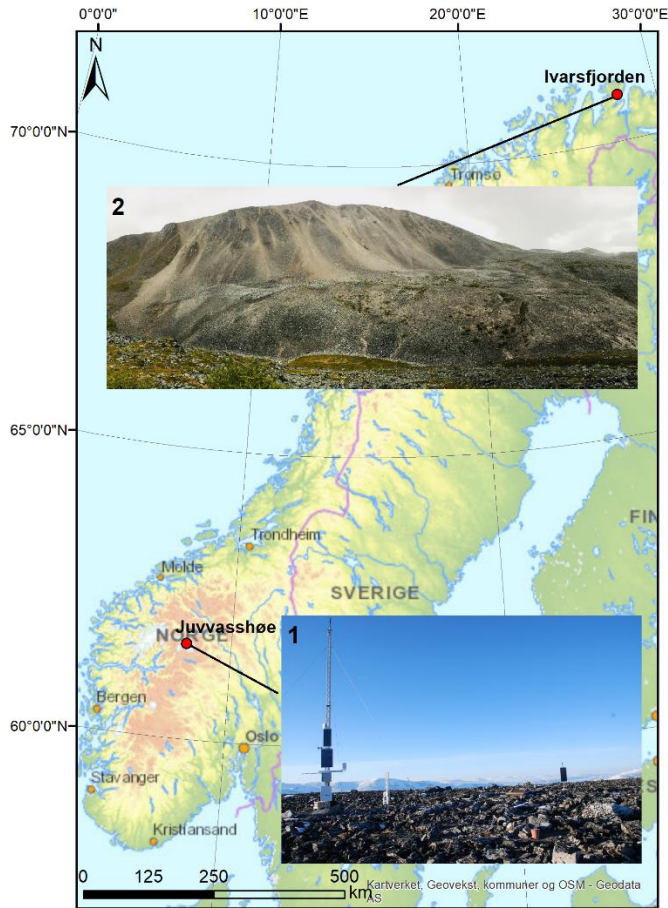
135 In this study, we present CryoGrid simulations of the coupled heat and water/ice balance for blocky terrain in Norway
136 and evaluate the impact of the ground stratigraphy and the drainage regime on ground temperatures and ice content for different
137 idealized subsurface stratigraphies and drainage regimes using CryoGrid, applied at. The model is set up with forcing data for
138 two Norwegian permafrost sites-, namely a blockfield site in the high mountains in southern Norway and a rock glacier site
139 near sea level in northern Norway. The aim is to contribute to an improved process understanding of the coupled subsurface
140 energy and water/ice balance, focusing on the observed. The employed model scheme does not account for air movement and
141 rocks protruding the snow cover as the “classic” causes for the negative thermal anomaly in coarse, blocky deposits. In
142 particular, we present simulations how the ground ice mass balance of blocky terrain, but is capable of simulating the seasonal
143 dynamics of the ground ice table in blocky terrain. The goal of the study is to evaluate to what extent the thermal anomaly in
144 blocky terrain can affect ground temperatures and the occurrence of permafrost be simulated by such a comparatively simple
145 scheme which could in principle be integrated in larger-scale permafrost modelling and mapping efforts. In particular, we
146 investigate the interplay with the seasonal snow cover and discuss the impact on the permafrost distribution in mountain
147 environments.

148 2 Study sites

149 2.1 Juvvasshøe, southern Norway

150 Juvvasshøe (61°40 N, 08°22 E, 1894 m.a.s.l.) (Fig. 1) is a site located in Jotunheimen in the southern Norwegian mountains,
151 Jotunheimen well above the tree line. A 129 m deep borehole was drilled in August 1999 in the PACE (Permafrost and Climate
152 in Europe) project (Harris et al., 2001). Continuous data streams from this PACE borehole are available with the exception of
153 a gap between 21 December 2011 to 24 April 2014. The site is located in an extensive block field on a mountain plateau with
154 sparse vegetation cover. The bedrock (crystalline rocks, Farbroten et al., 2011) is located at approximately 5 m depth, the first
155 meter consists of large stones and boulders and the ground below mainly consists of cobbles (Isaksen et al., 2003). Between
156 2000 and 2004, Isaksen et al. (2007) measured a mean annual air temperature (MAAT) at 2 m height of -3.3 °C. The mean
157 ground temperature (MGT) at 2.5 m below the surface during this period was -2.5 °C. The mean annual precipitation was
158 estimated to be between 800 and 1000 mm-yr⁻¹. The site is extremely wind-exposed, resulting in a low snow thickness due to
159 wind drift. Hipp et al. (2012) described a snow depth of less than 20 cm, while the snow thickness in surrounding, lower-lying
160 and less exposed sites can be up to 140 cm. Isaksen et al. (2007) measured the difference between the mean annual ground
161 surface temperature (MAGST) and mean annual air temperature (MAAT(-)), which is the surface offset, at exposed and less
162 exposed sites in this area. At sites with a significant snow cover, the surface offset was more than 2 °C, while at exposed
163 (including Juvvasshøe) sites this offset is generally below 1 °C. The permafrost thickness at the PACE borehole was estimated

164 to be approximately 380 m (Isaksen et al., 2001), with the lower permafrost limited at ca. 1450 m.a.s.l. (Farbrot et al., 2011).
165 The thickness of the active layer increased from 215 cm in 1999 (Isaksen et al., 2001) to ca. 250 cm in 2019 (Etzelmüller et
166 al., 2020). A weak zero curtain effect suggests a low water content in the active layer (Isaksen et al., 2007). A warming of 0.2
167 °C per decade and 0.7 °C per decade in surface air temperature and ground surface temperature, respectively, occurred between
168 2000 and 2019 (Etzelmüller et al., 2020).



169
170 **Figure 1: Location of the two sites in Norway (© Norwegian Mapping Authority). (1) blockfield at Juvvasshøe (1894 m.a.s.l.), (2)**
171 **rock glacier at Ivarsfjorden (60–160 m.a.s.l.).**

172 2.2 Ivarsfjorden rock glacier, northern Norway

173 Ivarsfjorden is a small fjord arm of the larger Hopsfjorden, located on the Nordkinn peninsula in the Troms and Finnmark
174 county in northern Norway (Fig. 1). Deglaciated around 14–15 cal kyr BP (Romundset et al., 2011), the peninsula is dominated
175 by flat mountain plateaus of exposed bedrock, *in situ* weathered material and coarse grained till (LilleørenLilleøren et al.,
176 2022), which feature steep slopes towards the sea. The coastal areas of Finnmark have a wet maritime climate, with mean
177 annual precipitation around 1000 mm (Saloranta, 2012). Lilleøren et al. (2022) describe a MAAT of 1.6 °C between 2010 and

178 2019 in the area of the rock glacier. ~~The rock glacier of interest, which~~ lies in a southwest-northeast trending valley ~~that extends~~
179 ~~from the fjord and has at~~ an elevation extent of roughly 60 to 160 m_{r.a.s.l.}. The mountain at its east (443 m.a.s.l.) serves as the
180 source area with rockfall debris and coarse talus slopes being common. The bedrock in Ivarsfjorden consists of sandstones and
181 phyllites (NGU, 2008). Sandstones often generate coarse, bouldery material, which is favorable for the formation of rock
182 glaciers (Haeberli et al. 2006). The rock glacier in Ivarsfjorden is northwest facing and has previously been interpreted as relict
183 (Lilleøren and Etzelmüller, 2011), but a detailed analysis showed that a limited ice core might still be present (Lilleøren et al.,
184 2022). A negative MAAT around 100 to 150 years ago is an indication that rock glaciers in this area were likely active at the
185 end of the Little Ice Age (LIA). Refraction Seismic Tomography (RST) surveys indicate a porous air-filled stratigraphy such
186 as blocky talus deposits: at the near-surface at parts of the rock glacier. While observed MAGSTs between 2015 and 2020 are
187 all positive, negative surface temperatures during summer have been observed by a thermal camera at the front slope of the
188 rock glacier. This is likely an indication of the chimney effect and thus of connected voids that support air flow.

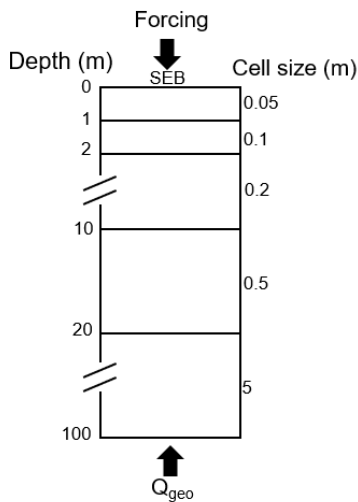
189 3. Methods

190 3.1 The CryoGrid community model

191 CryoGrid is a simulation toolbox for ground thermal simulations that can be applied to a wide range of applicationsmodelling
192 tasks in the terrestrial cryosphere thanks to its modular structure (see Westermann et al., 2022 for details). It hasis mainly been
193 applied in permafrost environments, using ~~heat conductionthe finite difference method~~ to transiently simulate ground
194 temperatures ~~transiently. To represent the energy and water cycle of.~~ We use a one-dimensional groundmodel column with a
195 domain depth of 100 m (as in the best possible way, CryoGrid allows the user to select different processes
196 representations/parameterizations for different vertical domains. As an example, a fully transient water balance can be used in
197 the near-surface region, whilee.g. Westermann et al., 2016; Schmidt et al., 2021) and grid cell sizes increasing with depth (Fig.
198 2). The lower boundary condition is provided by a constant geothermal heat flux. The upper boundary results from solving the
199 surface energy balance, including both radiative and turbulent heat fluxes, as well as the heat flux in the ground. In order to
200 compute the surface energy balance, atmospheric forcing data are required (Sect. 3.2). To calculate ground temperatures, both
201 conductive heat transfer following Fourier's law and advection of heat with vertically moving water is taken into account
202 (Westermann et al., 2022). The freezing characteristic of subsurface water/ice depends on the soil type, either following Painter
203 and Karra (2014) for sediments, or set to free water(ice) content is used in deeper layers. Likewise, different process
204 representations for the seasonal snow cover can be chosen. (water changes state at 0 °C, Westermann et al., 2022) for
205 subsurface material with large pores/voids, such as blocky terrain. To define the properties of the subsurface material, a
206 stratigraphy of -volumetric mineral, organic, water and ice eonentcontents and the field capacity (the ability to hold water
207 against gravity) must be provided (Westermann et al., 2022).

208 In the model setup used for this study, the lower boundary condition is provided by a constant geothermal heat flux
209 of 0.05 Wm⁻² which is a reasonable value for Norway used in previous modeling studies (Westermann et al., 2013). The upper

210 boundary results from solving the full surface energy balance, including both radiative and turbulent heat fluxes, which gives
211 rise to a ground heat flux. In order to solve the surface energy balance, atmospheric forcing data are required (chapter 3.4). A
212 scheme with heat conduction, following Fourier's law for heat conduction, and heat advection is used for heat transfer and
213 temperature calculation in the subsurface (Westermann et al., 2022).



214
215 **Figure 2: Schematic of the model grid, indicating cell sizes at different depths and upper and lower boundary conditions. As upper**
216 **boundary condition, the surface energy balance (SEB) forced by near-surface meteorological data is used. The lower boundary**
217 **condition is provided by a constant geothermal heat flux.**

218 For soil hydrology, a gravity driven bucket scheme is used (Westermann et al 2022). Rainfall is taken from provided
219 by the model forcing data and is added to the uppermost grid cell of, while evaporation is determined by the subsurface. The
220 surface energy balance calculations determine how the soil moisture is affected by evaporation. Transpiration plays no part in
221 this study as no vegetated (note that we consider unvegetated surfaces are involved and thus do not account for transpiration).
222 Water that is in excess of the field capacity infiltrates downwards until either the water table or a non-permeable layer, such
223 as a frozen grid cell is reached. The water table forms if excess water is available and cells are saturated from the bottom
224 upwards. If all grid cells are saturated, excess water is considered removed as surface runoff.

225 The freezing characteristic of water in the subsurface can be set to follow a freeze curve depending on the soil type,
226 following Painter and Karra (2014) or set as free water (water changes state at 0 °C, Westermann et al., 2022) for subsurface
227 material with large pores/voids, such as blocky terrain.

228 Studies that used a previous model version of CryoGrid (e.g. Westermann et al., 2013; Westermann et al., 2016;
229 Langer et al., 2016) assumed constant water/ice contents. This is a major limitation, as varying soil moisture contents strongly
230 affect the ground thermal regime (e.g. Martin et al., 2019). We use a one-dimensional model setup and, but simulate lateral
231 drainage out of the model domain water by assuming introducing a seepage face at atmospheric pressure. First, i.e. a lateral
232 boundary condition for water fluxes representing flow between the saturated grid cells of the model domain and a stream
233 channel (or the atmosphere) to which the water can freely flow out from the subsurface (e.g. Scudeler et al. 2017). Using the

234 elevation of the water table is calculated, after which a lateral water flux removes water in z_{wt} (computed as the elevation of
235 the uppermost saturated grid cell), lateral water fluxes F_i^{lat} are derived for all saturated unfrozen grid cells that are below
236 this the water table, following Eq. (1): (i.e. at elevations $z_i < z_{wt}$) as

$$237 F_i^{lat} = -K_H \frac{z_{wt} - z_i}{d^{lat}}, \quad (1)$$

238 where F_i^{lat} is the lateral water flux out of grid cell i , K_H is the saturated hydraulic conductivity, z_{wt} is the height of the water
239 table, z_i is the height of grid cell i and d^{lat} is the lateral distance to the seepage face. We use the and the flux is determined
240 by the difference between the hydrostatic potential (proportional to z_{wt}) of the water column and the gravitational potential of
241 free water at the elevation of each cell (proportional to z_i). Note that Eq. (1) is an approximation for small changes of the water
242 table and small outflow fluxes for which the potential in the saturated zone can be approximated by the hydrostatic potential.
243 The parameter d^{lat} is used to control the strength of the drainage, where low values result with small distances resulting in a
244 well-drained column and, while high values result in lead to suppressed drainage. In this study, we consider the two confining
245 cases with a poorly or completely undrained column. A small and large value of d^{lat} value of 10^4 m is used for undrained
246 cases, which emulates conditions at a mostly flat surface. In reality this, respectively (Sect. 3.3). In the former, water from rain
247 or ground ice melt is removed rapidly, effectively preventing the soil water from pooling up, while drainage is negligible in
248 the former, so that the setup corresponds to no drainage, resulting in a a classic one-dimensional case for the water balance,
249 where only surface water is removed. For the drained cases, a d^{lat} value of 1 m is used, which emulates well drained
250 conditions at a slope model scheme.

251 The snow model used in this study was introduced by Zweigel et al. (2021) and is based on the CROCUS Crocus
252 snow scheme (Vionnet et al. 2012, 2012) which accounts for snow microphysics and is designed to reproduce a realistic snow
253 pack structure (see Vionnet et al. 2012 for defining equations; Zweigel et al. 2021 for implementation in CryoGrid). Snowfall
254 is added on the surface with density and grain microphysical properties derived from atmospheric model forcing data, in
255 particular air temperature and then undergoes transient evolution of wind speed. The snow grains and density. The snow albedo
256 undergoes a transient evolution in this snow scheme. The physical effect of wind drift on the snowpack is included in the
257 module evolves due to compaction by the overburden pressure of overlying snow layers, as well. Energy as wind compaction
258 and mass transfer in the snowpack includes heat conduction, percolation refreezing of rainfall melt- and percolation of meltwater
259 (Westermann rainwater (Vionnet et al., 2022, 2012)). The amount of snow snowfall from the forcing data can be adjusted by a
260 so-called snowfall factor, sf , with which the snowfall rate from the model forcing is multiplied. With this, it is possible to the
261 effects of wind-induced snow redistribution on ground temperatures can be represented at least phenomenologically represent
262 redistribution of snow by wind (as in (Martin et al., 2019) and to account for potential biases in the snowfall forcing. In this
263 study, we conduct a sensitivity analysis towards the winter), using $sf < 1$ for areas with net snow cover by selecting different
264 values for sf .

265 Ground and snow parameters are kept constant in all model runs. For the ground we used an albedo of 0.15, emissivity
266 of 0.99, a roughness length of 10^{-3} m, ablation and a hydraulic conductivity of 10^{-5} m s⁻¹. For snow, we used an emissivity of
267 0.99, a roughness length of 10^{-3} m, a hydraulic conductivity of 10^{-4} m s⁻¹ if $f > 1$ and a field capacity of 0.05 (see Westermann et
268 al., ~~for areas~~ 2022).

269 **3.2 Validation, equilibrium and transient runs**

270 Three types of CryoGrid simulations are distinguished, i.e. *validation runs*, *equilibrium runs* and *transient runs*. The
271 *validation runs* are set up to compare modelled ground temperatures with available field measurements at the two sites. At
272 Juvvasshøe, measurements consist of borehole data from 2000 to 2019, allowing a comparison at different depths. At the rock
273 glacier in Ivarsfjorden, comparison of model results with in situ measurements is accomplished with the available ground
274 surface temperature monitoring network (Lilleøren et al., 2022), using the loggers within the rock glacier outline and with
275 continuous measurements. The *equilibrium runs* aim to investigate the effect of three idealized stratigraphies under a range of
276 different amounts of snowfall on the ground thermal regime and ground ice table for a stable climate, using looped model
277 forcing from the years 2000–2010 at Juvvasshøe and 1960–1970 at the Ivarsfjorden rock glacier. Each stratigraphy is modelled
278 for both the *undrained* and *drained* cases, resulting in six scenarios. The goal of the *transient runs* is to analyze how the ground
279 temperatures and ground ice table may have developed from 1951 to 2019 under these different model setups net deposition.

280 **3.3 Ground stratigraphy and snow**

281 The porosity Downscaling of the ground material and the thickness of sediment are important factors for the capacity of the
282 ground to hold water. Three idealized ground stratigraphies are set up in order to investigate the effect of water drainage on
283 the ground thermal regime and ground ice dynamics. ~~These are referred to as the *blocks only*, *blocks with sediment* and *sediment*~~
284 ~~*only* stratigraphies (Table 1) in the following.~~ In all stratigraphies, bedrock is assumed below 5 m depth. Also, the bedrock
285 properties of 3% porosity and saturated conditions are kept constant throughout the study, which is in agreement with Hipp et
286 al. (2012) and Farbrøt et al. (2011).

287 The *blocks only* stratigraphy consists of a coarse block layer with 50% porosity of 5 m thickness on top of bedrock.
288 The coarse blocks have a low field capacity of 1% (Table 1), which means that almost all water drains first downwards and
289 then laterally for the drained case. This idealized stratigraphy roughly corresponds to an active rock glacier where finer
290 sediments that result from weathering and erosion processes are transported towards the tongue of the rock glacier.
291 Furthermore, Dahl (1966) observed that blockfields on slopes more often do not contain a fine sediment fraction between the
292 blocks in northern Norway. In the second stratigraphy, *blocks with sediment*, the voids between coarse blocks are filled by a
293 finer-grained sediment fraction (sand) with again 50% porosity, resulting in an overall porosity of 25% and a higher field
294 capacity as water is held in the finer pores of the sediment fraction. Finally, the *sediment only* stratigraphy contains sand with
295 the same porosity as *blocks only*, but a higher field capacity again due to the water holding capacity of the fine-grained sediment
296 material.

297

298 **Table 1. Three idealized subsurface stratigraphies. The values indicate the volumetric fractions of the soil constituents.**

Depth (m)	Mineral	Organic	Porosity	Field capacity	Soil freezing
<i>Blocks only</i>					
0-5	0.5	0.0	0.5	0.01	Free water
<i>Blocks with sediment</i>					
0-5	0.75	0.0	0.25	0.15	Free water
<i>Sediment only</i>					
0-5	0.5	0.0	0.5	0.25	Sand

299

300 A changing snow cover is the main source of spatial variability in ground temperatures in Norwegian mountains
 301 (~~Cisnås et al., 2016~~). Following these studies, the sensitivity of the scenarios to different amounts of snowfall. All model runs
 302 use the same snow model, but the snowfall factor *sf* is adjusted to change the thickness of the winter snowpack.

303 *Validation runs.* For the validation runs with the borehole data in Juvvasshøe, different stratigraphies were manually
 304 tested until a good visual fit between modelled and measured ground temperatures at 2.0 m and 0.4 m depth was established.
 305 Based on observations of blocks and smaller cobbles with finer sediments down to the onset of bedrock at a depth of 5 m
 306 (Isaksen et al. 2003), the *blocks with sediment* stratigraphy is used as a starting point and the mineral content is increased in
 307 order to achieve a better fit. ~~As this site is extremely exposed to wind and most snow is blown away (Isaksen et al. 2003;~~
 308 ~~Westermann et al., 2013), the snowfall factor is set to values smaller than 1.~~ The stratigraphies used for comparison to field
 309 measurements at the rock glacier in Ivarsfjorden are the *blocks with sediment* and *sediment only*, in addition to a two-layered
 310 blockfield stratigraphy used in a previous modeling study on ground temperatures in blockfields (see Table 1, Westermann et
 311 al., 2013). All loggers except for one are placed on the relict surface of the rock glacier (Lilleøren et al., 2022), where the
 312 surface does not consist of just coarse blocks, but also contains finer sediment in between. Here, the *blocks with sediment* and
 313 *sediment only* stratigraphy are considered most appropriate.

314 *Equilibrium runs.* The equilibrium runs simulate the equilibrium ground temperature for the three idealized
 315 stratigraphies in both the *drained* and *undrained* case. For each scenario, CryoGrid is run with snowfall factors of 0.0, 0.25,
 316 0.5, 0.75, 1.0 and 1.5. This approach allows for an estimation of the threshold amount of snow above which permafrost will
 317 no longer exist in each of the six scenarios. Note that for all snowfall factors in this study, the snow pack fully melts in all
 318 years; only for *sf* values exceeding 2 at Juvvasshøe, the snowpack survives the summer in some years, eventually forming a
 319 perennial snow/ice patch.

320 *Transient runs.* The same three idealized stratigraphies are used to simulate the transient change in ground temperature
 321 and ground ice content over the period 1951 to 2019. This allows to investigate the susceptibility to ground warming/thawing

322 in a period when a significant increase air temperatures occurred at the two sites. For each of the sites, the best fitting snowfall
323 factor from the validation runs is chosen for the transient analysis.

324

325 **3.4 Model forcing**

326 The meteorological data used to force the CryoGrid model were generated by applying TopoSCALE, a topography-based
327 downscaling routine (Fiddes and Gruber, 2014), to ERA5 reanalysis data (Hersbach et al., 2020). TopoSCALE is employed in
328 cryosphere applications in complex terrain, including estimating mountain permafrost distribution (Fiddes et al., 2015), snow
329 data assimilation (Aalstad et al., 2018; Fiddes et al., 2019), and downscaling regional climate model output (Fiddes et al.,
330 2022). ~~ERA5 outputs are~~ ERA5 output is provided as interpolated point values on a regular latitude-longitude grid at a
331 resolution of 0.25° at an hourly frequency, both at the surface level, corresponding to Earth's surface as represented in the
332 reanalysis, and at 37 pressure levels in the atmosphere from 1000 to 1 hPa. We considered data for the reanalysis period from
333 1951 to 2019. ~~From~~ at three-hourly resolution. As input to TopoSCALE, we obtained from the surface level ~~we obtained:~~ 2
334 meter air and dewpoint temperature, 10 meter meridional (northward) and zonal (eastward) wind velocity components, surface
335 pressure, constant surface geopotential, incoming longwave radiation, incoming shortwave radiation, and total precipitation.
336 From the pressure levels we acquired: air temperature, specific humidity, zonal and meridional wind velocity components, and
337 dynamic geopotential. For Juvvasshøe at 1894 m a.s.l. we used all levels in the range 900 hPa to 700 hPa, while for the lower
338 elevation Ivarsfjorden rock glacier at 60–160 m a.s.l. we used all levels between 900 hPa and 1000 hPa.

339 ~~Terrain parameters derived from~~ To account for terrain shading in the downscaling routine, a digital elevation model
340 (DEM) ~~are needed to apply topography-based downscaling to the ERA5 data. We obtained these parameters by processing~~ is
341 required, for which we use the mosaic version of the ArcticDEM with a resolution of 32 m (Porter et al., 2018) at ~~the~~
342 ~~respective~~ both sites. ~~Based on the ERA5 data and the DEM-derived parameters we performed a topography-based downscaling~~
343 ~~using the TopoSCALE routine. TopoSCALE is routinely used to downscale atmospheric reanalysis data in complex terrain~~
344 ~~and has since been used in several cryospheric applications including estimating mountain permafrost distribution (Fiddes et~~
345 ~~al., delivers 2015), snow data assimilation (Aalstad et al., 2018), hyper-resolution snow reanalysis (Fiddes et al., 2019), and~~
346 ~~downscaling regional climate model output (Fiddes et al., 2022).~~
347 ~~By applying TopoSCALE all the necessary meteorological forcing fields~~ data required to run CryoGrid ~~are retrieved:~~ near
348 surface air temperature, specific humidity, wind speed, incoming longwave radiation, incoming shortwave radiation, as well
349 as snowfall and rainfall.

350 **3.53 Model initialization setup**

351 Three idealized ground stratigraphies are set up in order to investigate the effect of water drainage on the ground thermal
352 regime and ground ice dynamics in blocky terrain. These are referred to as the *blocks only*, *blocks with sediment* and *sediment*
353 only stratigraphies (Table 1) in the following. The *blocks only* stratigraphy consists of a coarse block layer with 50% porosity

354 and air-filled voids which is assigned low field capacity of 1% (Table 1), i.e. the surfaces of the coarse blocks retain only little
 355 water. This idealized stratigraphy is designed to represent an active rock glacier where finer sediments resulting from
 356 weathering and erosion processes are transported towards the tongue of the rock glacier. Furthermore, Dahl (1966) observed
 357 that blockfields on slopes more often do not contain a fine sediment fraction between the blocks in northern Norway, so that
 358 the *blocks only* stratigraphy can also represent active blockfields. The second stratigraphy, *blocks with sediment*, is designed
 359 to represent blocky terrain where the voids are filled by finer sediments. This is often observed in blockfields on more flat
 360 surfaces, which are more likely to retain finer sediment within their pores (as in Isaksen et al., 2003 and Dahl 1966). We again
 361 consider coarse blocks with 50% porosity (as for the *blocks only* stratigraphy), but as the voids are filled with fine sediments
 362 (which again are assumed to have 50% porosity), the overall porosity is only 25%. Furthermore, a significantly higher field
 363 capacity than for the *blocks only* stratigraphy is assigned as more water can be held in the finer pores of the sediment fraction.
 364 Finally, the *sediment only* stratigraphy serves as a control scenario for a soil without blocks. It contains sediment with 50%
 365 porosity and a high field capacity due to the water holding capacity of the fine-grained sediment material. For all stratigraphies,
 366 bedrock (3% porosity and saturated conditions, e.g. Hipp et al. 2012; Fabrot et al. 2011) is assumed below 5 m depth, which
 367 is in line with observations from Isaksen et al. (2003) at Juvvasshøe. Finally, none of the stratigraphies contain soil organic
 368 matter. We emphasize that the stratigraphies are in qualitative agreement with field observations of air and sediment-filled
 369 block layers in Norway, but the assumed porosities of 50% for both the block layer and the sediments represent idealized
 370 scenarios. However, we perform a sensitivity analysis for different porosity values (see Supplement) to investigate the impact
 371 of this parameter on the simulation results.

372
 373 **Table 1: Mineral content, porosity, field capacity (all in vol. fraction) and soil freezing characteristic for the three idealized**
 374 **subsurface stratigraphies.**

<u>Name</u>	<u>mineral</u>	<u>porosity</u>	<u>field capacity</u>	<u>soil freezing characteristic</u>
<u><i>Blocks only</i></u>	<u>0.5</u>	<u>0.5</u>	<u>0.01</u>	<u>Free water</u>
<u><i>Blocks with sediment</i></u>	<u>0.75</u>	<u>0.25</u>	<u>0.15</u>	<u>Free water</u>
<u><i>Sediment only</i></u>	<u>0.5</u>	<u>0.5</u>	<u>0.25</u>	<u>Sand</u>

375
 376 For the geothermal heat flux lower boundary condition, a value of 0.05 Wm⁻² is used, which is a typical value for Norway used
 377 in previous modelling studies (Westermann et al., 2013).

378 To investigate the effect of subsurface drainage on ground temperatures and ground ice conditions, we distinguish *undrained*
 379 and *drained* scenarios by using two different values of d^{lat} (Eq. 1) for in the idealized stratigraphies. A d^{lat} value of 10⁴ m is
 380 used for *undrained* cases, which emulates conditions at a flat surface, resulting in a to a good approximation one-dimensional
 381 water balance, where only surface water is removed. For the *drained* cases, a d^{lat} value of 1 m is used, which results in well-

382 drained conditions which are typical in sloping terrain. For the saturated hydraulic conductivity K_H , a fixed value of 10^{-5} m s^{-1}
 383 is used for all stratigraphies, although the true hydraulic conductivities almost certainly differ between stratigraphies.
 384 However, the key parameter controlling lateral water fluxes in Eq. 1 is in reality the “drainage timescale” $K_H/d^{lat} [\text{s}^{-1}]$, which
 385 is varied by four orders of magnitude between $K_H/d^{lat} = 10^{-5} \text{ s}^{-1}$ ($d^{lat} = 1 \text{ m}$, well-drained conditions) and $K_H/d^{lat} = 10^{-9} \text{ s}^{-1}$
 386 ($d^{lat} = 10^{-4} \text{ m}$ undrained conditions). As the study setup is designed to analyze these two “confining cases”, it is sufficient to
 387 only vary d^{lat} and leave K_H constant for simplicity. Further sensitivity tests for d^{lat} and K_H are provided in the
 388 Supplement. With the exception of the *snowfall factor* (see Sect. 3.3.1 to 3.3.3), the parameters in the snow model are kept
 389 constant in all model runs, using a surface emissivity of 0.99, a roughness length of 10^{-3} m , a saturated hydraulic conductivity
 390 of 10^{-4} m s^{-1} and a field capacity of 0.05 (Westermann et al. 2022). For the ground surface, we used an albedo of 0.15, emissivity
 391 of 0.99, and a roughness length of 10^{-3} m .

392 We perform three types of model simulations which differ in their overall purpose. For *validation* runs (Sect. 3.3.1), we adjust
 393 subsurface stratigraphy and *snowfall factor* in order to compare model results with the available field measurements from the
 394 two study site. *Equilibrium* runs (Sect. 3.3.2) and *transient* runs (Sect. 3.3.3) are designed to explore the sensitivity of the
 395 simulated ground thermal regime towards the three idealized stratigraphies (Table 1) and the two drainage cases. An overview
 396 of the basic settings of the different simulation types is provided in Table 2.

397

398 **Table 2: Overview of basic model settings for the different simulation types. A spin-up of subsurface temperatures is achieved by**
 399 **repeated simulations for the spin-up period (until a stable temperature profile is reached), before the actual model run for the**
 400 **simulation period is conducted. “Idealized” stratigraphy and drainage refers to three subsurface stratigraphies (Table 1) combined**
 401 **with two types of drainage conditions. See Sect. 3.3.1 to Sect. 3.3.3 for details.**

<u>Simulation type</u>	<u>Site</u>	<u>Spin up period</u>	<u>Simulation period</u>	<u>Stratigraphy and drainage</u>	<u>Snowfall factor</u>
<u><i>Validation</i></u>	<u>Juvvasshøe</u>	<u>1951-2010</u>	<u>2010-2019</u>	<u>Best-fit</u>	<u>0.25</u>
	<u>Ivarsfjorden</u>	<u>1951-2016</u>	<u>2016-2019</u>	<u>Best-fit</u>	<u>1</u>
<u><i>Equilibrium</i></u>	<u>Juvvasshøe</u>	<u>2000-2010</u>	<u>2000-2010</u>	<u>Idealized</u>	<u>0.0, 0.25, 0.5, 0.75, 1.0, 1.5</u>
	<u>Ivarsfjorden</u>	<u>1962-1971</u>	<u>1962-1971</u>	<u>Idealized</u>	<u>0.0, 0.25, 0.5, 0.75, 1.0, 1.5</u>
<u><i>Transient</i></u>	<u>Juvvasshøe</u>	<u>1962-1971</u>	<u>1951-2019</u>	<u>Idealized</u>	<u>0.25</u>
	<u>Ivarsfjorden</u>	<u>1962-1971</u>	<u>1951-2019</u>	<u>Idealized</u>	<u>1</u>

402

403 3.3.1 Validation runs

404 As a prerequisite for conducting model experiments on ground stratigraphy and drainage (Sects. 3.3.2, 3.3.3), validation runs
405 are set up to show that the model can reproduce key characteristics of the thermal regime at the two sites in a satisfactory
406 manner (based on available observations). Furthermore, we use the observations to determine the best-fitting *snowfall factor*
407 for the two sites which is subsequently used in the transient runs (Sect. 3.3.3). At Juvvasshøe, temperature measurements in a
408 borehole are available from 2000 to 2019, allowing a comparison at different depths. At the Ivarsfjorden rock glacier site,
409 observations of ground temperature at deeper depths are lacking, but measurements of near-surface ground temperatures are
410 available from July 2016 to July 2019 (Lilleøren et al., 2022). These are compared to simulation results to ensure that the
411 model reproduces the observed surface offset between air and ground surface, largely caused by the winter snow cover (e.g.
412 Martin et al., 2019; Schmidt et al., 2021). At both sites, the model is ran for the entire period of available forcing data, leaving
413 at least 60 years for the model spin-up which is sufficient to analyze ground temperatures in uppermost meters of the ground
414 column.

415 Manual adjustment of the ground stratigraphy (porosity and thus mineral content) and snowfall factor are performed until a
416 good fit with daily measurements is achieved. At Juvvasshøe, based on observations of blocks and smaller cobbles with finer
417 sediments down to the onset of bedrock at a depth of 5 m (Isaksen et al. 2003), the *blocks with sediment* stratigraphy is used
418 as a starting point to vary porosities until a good fit is achieved. As this site is extremely exposed to wind and most snow is
419 blown away (Isaksen et al. 2003; Westermann et al., 2013), the snowfall factor is ~~For the validation runs both at Juvvasshøe~~
420 and Ivarsfjorden, the model is run for the entire period of available forcing data. At Juvvasshøe the initial ground temperature
421 profile is taken from the borehole data. At Ivarsfjorden the model is initialized to near-equilibrium conditions with the first 10
422 years of available forcing data. At Juvvasshøe, we compare the years 2010 to 2019 to measurements, while 2016 to 2019 is
423 used for Ivarsfjorden. This leaves at least 60 years for the model spin up which is sufficient to analyze ground temperatures in
424 uppermost meters of the ground column.

425 In order to reach steady state conditions in the ~~stepwise decreased to values below one to improve~~improve the model
426 performance. At Ivarsfjorden, we considered 11 temperature loggers within the rock glacier outline (Fig. 1d in Lilleøren et al.,
427 2022), of which all except for one are placed on the relict surface of the rock glacier (Fig. 2a in Lilleøren et al., 2022). On the
428 relict surface, deposition of finer sediment in between blocks is more likely than on the active surface, due to the lack of
429 movement. Here, the *blocks with sediment* stratigraphy is considered appropriate and used as starting point for the calibration.
430 At both sites, the root-mean-square-error (RMSE) and bias are calculated in order to provide an objective measure of the model
431 fit. At Juvvasshøe this was accomplished for daily values at 0.4 m and 2 m depth, while at Ivarsfjorden the mean daily ground
432 surface temperature of the loggers within the rock glacier outline is used.

433 3.3.2 Equilibrium runs

434 The goal of equilibrium runs is to investigate the sensitivity of the ground thermal regime towards ground properties
435 and drainage conditions, using both the *undrained* and *drained* setup for the three idealized stratigraphies (Table 1) which
436 results in six scenarios. As the heavily wind-affected snow cover is a key source of spatial variability in ground temperatures
437 in the Norwegian mountains (Gisnås et al., 2014; Gisnås et al., 2016), the model is run for a range of snowfall factors between
438 0.0 and 1.5 (Table 2) for each scenario. This analysis allows us to identify the magnitude of the thermal anomaly that the
439 subsurface drainage induces at various amounts of snow, as well as estimate the threshold snow amount for permafrost
440 existence in the six scenarios. This analysis is performed for equilibrium runs, a conditions for 10 year period periods of roughly
441 stable climate, which is chosen and iterated three times until a steady state temperature profile of the uppermost 5 meters
442 is established. For Juvvasshøe, the period 2000–to 2010 is selected as the model can be initialized with real-time borehole
443 data. For the Ivarsfjorden steady-state runs, the comparatively cold period 1960–1970 1962 to 1971 is selected as this relatively
444 stable period is more likely to represent permafrost conditions than the other periods.

445 The goal of the transient runs is to investigate the warming and possible degradation of permafrost and ground ice melt from
446 the second half of the 20th century until present for the different model scenarios, so that the rates of warming/thawing can be
447 compared. For this purpose, an initialization procedure that allows the build-up of a stable ground ice table is required. This is
448 achieved by iterating three times over the coldest 10 year period in the forcing data, from 1962 to 1971, until equilibrium
449 conditions with a stable ice table are present. This is the coldest period in the available forcing data and thus the closest to
450 Little Ice Age climate conditions, when the rock glacier Ivarsfjorden is hypothesized to have been rock glacier was very likely
451 active (Lilleøren et al., 2022). Steady state

452 3.3.3 Transient runs

453 The goal of the transient runs is to analyze the effect of ground stratigraphies and drainage conditions on the transient response
454 of ground temperatures and ice tables to climate warming. For this purpose, we perform model simulations for this
455 initialization from 1951 to 2019, when air temperatures have increased by more than 1°C in Norway. To initialize simulations,
456 we perform a model spin-up by iterating three times over the coldest 10 year period are then followed by the transient in the
457 forcing data (1962 – 1971) which is sufficient to achieve a stable ice table. This is the same period as in the equilibrium runs
458 (see Sect. 4), for which it was selected to capture permafrost conditions at the Ivarsfjorden rock glacier site (see Sect. 4). Thus,
459 the transient runs allow us to analyze the evolution of the permafrost towards the warming of the recent decades. We only use
460 the best fitting snowfall factor (Table 2), as derived from the validation runs (Sect. 3.3.1), but again perform simulations for
461 the entire forcing dataset from 1951 to 2019. Transient runs three idealized stratigraphies and *undrained* and *drained* conditions.
462 This way, we can evaluate whether different ground stratigraphies or drainage conditions lead to different warming rates of
463 ground temperatures, as well as different thresholds for Juvvasshøe are set up by the same procedure, using the coldest period
464 1962 to 1971 for spin-up permafrost thaw.

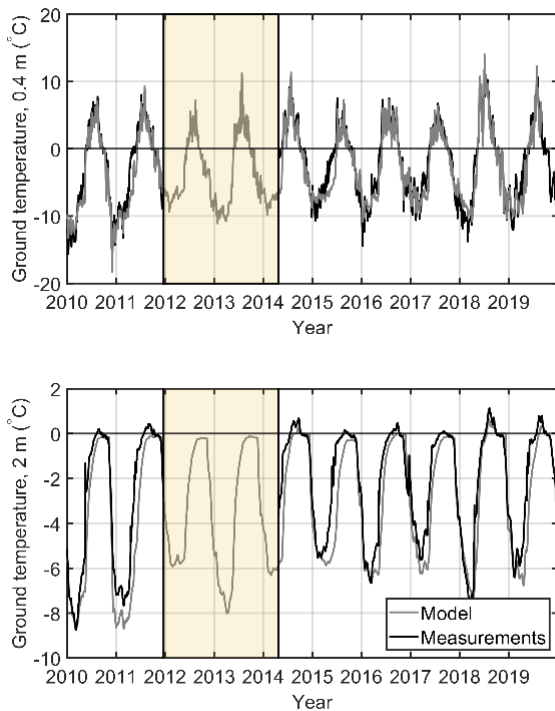
465 4. Results

466 4.1 Comparison to in-situ measurements

467 ~~Model~~The results of the *validation runs* at Juvvasshøe are compared with measured daily ground temperatures at the PACE
468 borehole (Etzelmüller et al, 2020). Figure ~~23~~ shows the comparison of measured ground temperatures with modelled
469 temperatures at ~~2-m~~0.4 and 2.0-4 m depth for the best fitting model configuration. The snowfall factor for this model setup is
470 0.25, ~~meaning the model reduces i.e.~~ incoming ~~snow~~snowfall is reduced by 75% in order to capture the effect of snow ablation
471 due to wind drift. This resulted in mean annual maximum snow depths of 34 cm, in broad agreement with observations from
472 the site (Iskasen et al., 2003) and earlier modeling studies at the site (Westermann et al., 2013). The subsurface stratigraphy
473 for ~~the best fitting this~~ model configuration is highly similar to the *blocks with sediment* stratigraphy, but with a slightly lower
474 porosity of 0.2 (i.e. a volumetric mineral content of 0.8) ~~and an accordingly lower field capacity of 0.1.~~ This would for
475 example correspond to blocks and cobbles with a porosity of 0.4 (0.5 for *blocks with sediment*), filled with fine sediments with
476 a porosity of 0.5 (and field capacity 0.25), which is plausible given the broad characteristics of the observed borehole
477 stratigraphy (Isaksen et al., 2003). ~~At 2 m depth, the simulations have a slight cold bias for the annual maxima close to 0 °C.~~
478 ~~The model simulates temperatures at 2 m depth better than at 0.4 m depth, as the effect of the strong variability of the ground~~
479 ~~surface temperature likely due to variations in the snow cover is dampened.~~ This configuration used *drained conditions*,
480 ~~although differences with undrained conditions are minimal for this stratigraphy. For daily temperatures at 0.4 m depth, the~~
481 ~~RMSE and bias are 2.1 °C and -0.6 °C, respectively, while they are 1.2 °C and -0.7 °C at 2 m depth. There is a mismatch in~~
482 ~~the timing of spring temperatures at 2 m depth in several years, for which modelled temperatures increase later than measured~~
483 ~~values. This is likely a result of differences in the snow melt, as the snowpack dynamics resulting from wind redistribution is~~
484 ~~not completely captured by the snowfall scaling with a constant snowfall factor (e.g. Martin et al., 2019).~~ Furthermore, the
485 uppermost 1 m contain large stones and boulders, while the layer below is characterized by smaller stones and cobbles; (Isaksen
486 et al. 2003), so that a ~~stratigraphic model~~ground stratigraphy with two layers in the uppermost 5 m ~~might possibly yield an~~
487 ~~even better fit~~ may further improve the performance of the simulations.

488

489



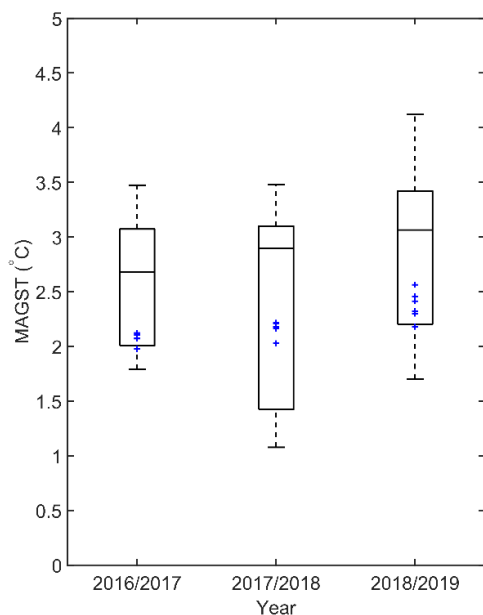
490

491 **Figure 23:** Modelled and measured ground temperature at the PACE borehole in Juvvasshøe at 0.4 m (upper) and 2.0 m (lower)
 492 depth. The shaded area indicates a period when no borehole data are available.

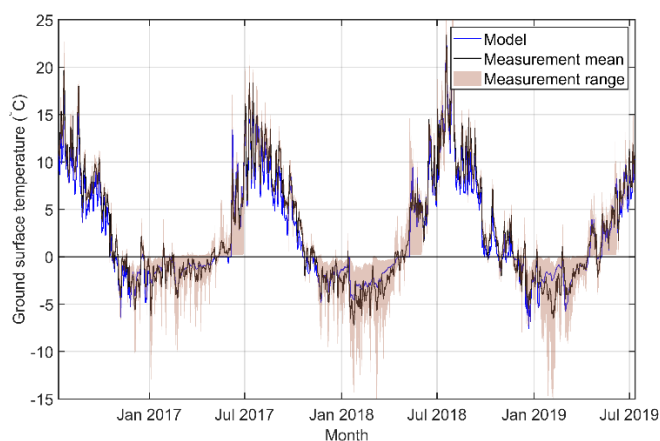
493 At the rock glacier in Ivarsfjorden, ~~no borehole data are available. Therefore,~~ a comparison between modelled and
 494 measured temperature is performed ~~with data from a ground surface temperature logger network (Lilleøren et al., 2022). As~~
 495 ~~this site is characterized by complex microtopography with likely strong variability of the snow cover (for which no~~
 496 ~~observations are available), we focus on mean annual average daily~~ ground surface temperatures (MAGST) for individual years
 497 ~~instead of a time-resolved comparison as for Juvvasshøe. The three years of data at 11 locations on and near the rock glacier~~
 498 ~~are presented together with six model validation runs (Fig. 3). These consist of two idealized stratigraphies (Sect. 3.3), in~~
 499 ~~addition to the blockfield stratigraphy (see Table 1, Westermann et al., 2013) each in a drained and undrained configuration~~
 500 ~~with a snowfall factor 1.0. There is likely a variable snow depth across the different parts of the rock glacier, which possibly~~
 501 ~~explains part of the differences between modelled and measured temperatures.~~

502 Measured MAGST are in the range of 1.1 °C and 4.1 °C, while modelled MAGST are confined in a narrower range
 503 between 2.0 °C and 2.7 °C. For all years combined, using the mean of the measurements is 2.7 °C, while the mean of all model
 504 realizations is 2.2 °C. We emphasize that the simulations all use a single snowfall factor and identical surface at 11 sites within
 505 the rock glacier as target for the comparison (Fig. 4). The best-fitting model configuration was found to be the blocks with
 506 sediment stratigraphy and a snowfall factor of 1.0, resulting in an RMSE of 1.3 °C and a bias of -0.4 °C. As in Juvvasshøe, the
 507 configuration used drained conditions, which likely explains the smaller range of simulated temperatures. In reality, the loggers

508 are distributed in an area where while differences with *undrained* conditions are small-scale spatial variations in topography,
509 snow accumulation, ground stratigraphy and vegetation play a role. Fig. 4 also shows the significant spatial variability of
510 ground surface temperatures, which is particularly large in winter. Also in periods, when the simulation results and the mean
511 of the measurements visibly deviate, the simulations remain within the range of the measurements. While there are some
512 deviations between ~~measurements~~ the observations and simulation results at both Juvvasshøe and Ivarsfjorden, we conclude
513 that the model setup (including the model forcing) can capture the general ground surface temperature regime at both sites
514 which is a prerequisite for obtaining meaningful results from the *equilibrium* and *transient runs*.



515



516

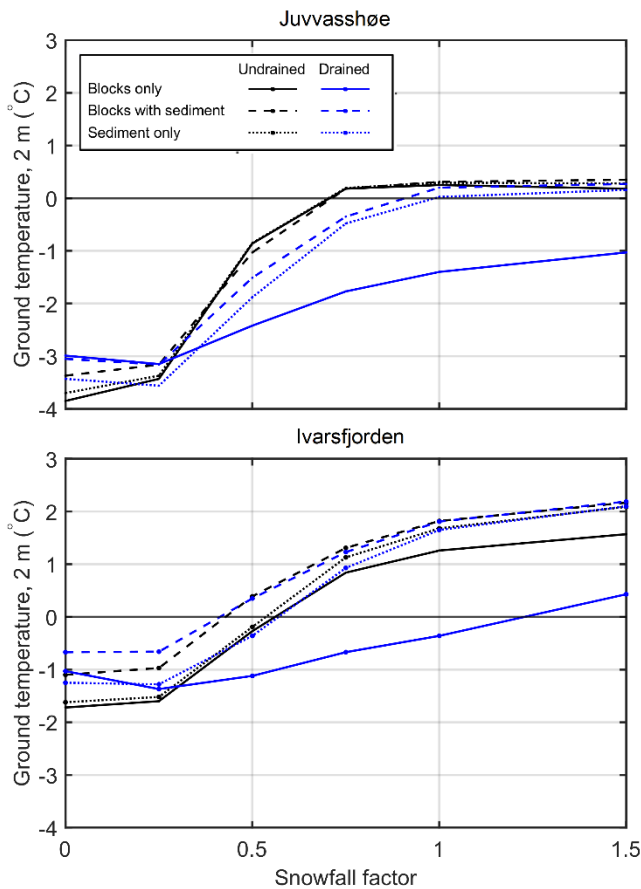
517 **Figure 3: Modelled and measured MAGST ground surface temperatures in Ivarsfjorden during three years, from**
518 **13 July 2016 to 12 July 2019. The bars indicate the 25th and 75th percentile of measured MAGST and shaded area indicates the**

519 whiskers represent the minimum to maximum and minimum temperatures. The blue indicators show modelled MAGST during the
520 same period for a selected range of ground stratigraphies at $sf = 1$ range of measured daily values from 11 loggers (based on Lilleøren
521 et al., 2022), while the black line represents the mean value of all loggers.

522

523 4.2 Equilibrium ground temperatures and sensitivity to snow

524 Annual maximum snow depths at a snowfall factor of 1.0 are between 1.5 m and 2.4 m at Juvvasshøe and between 0.4 m and
525 1.0 m at Ivarsfjorden. Figure Fig. 4 shows the equilibrium average ground temperature at 2 m depth for the three stratigraphies
526 at, the drained and the undrained scenario, and different snowfall factors at both sites. For each of the three stratigraphies there
527 is the drained and the undrained scenario. At both sites there is a clear pattern of lower temperatures in the *blocks only, drained*
528 scenario (solid blue line) compared to all five other scenarios. For snowfall factors of 0.75 and larger, the difference in ground
529 temperature between *blocks only, drained* and the other scenarios is in the range of 1.1 °C and 1.8 °C at Juvvasshøe and in the
530 range of 1.1 °C and 2.2 °C at Ivarsfjorden. This shows that the magnitude of the negative thermal anomaly increases with a
531 larger amount of snowfall. Results of the sensitivity study to porosity of the soil (see Supplement) show that mean ground
532 temperatures are within 0.4 °C between the highest and lowest porosity tested.

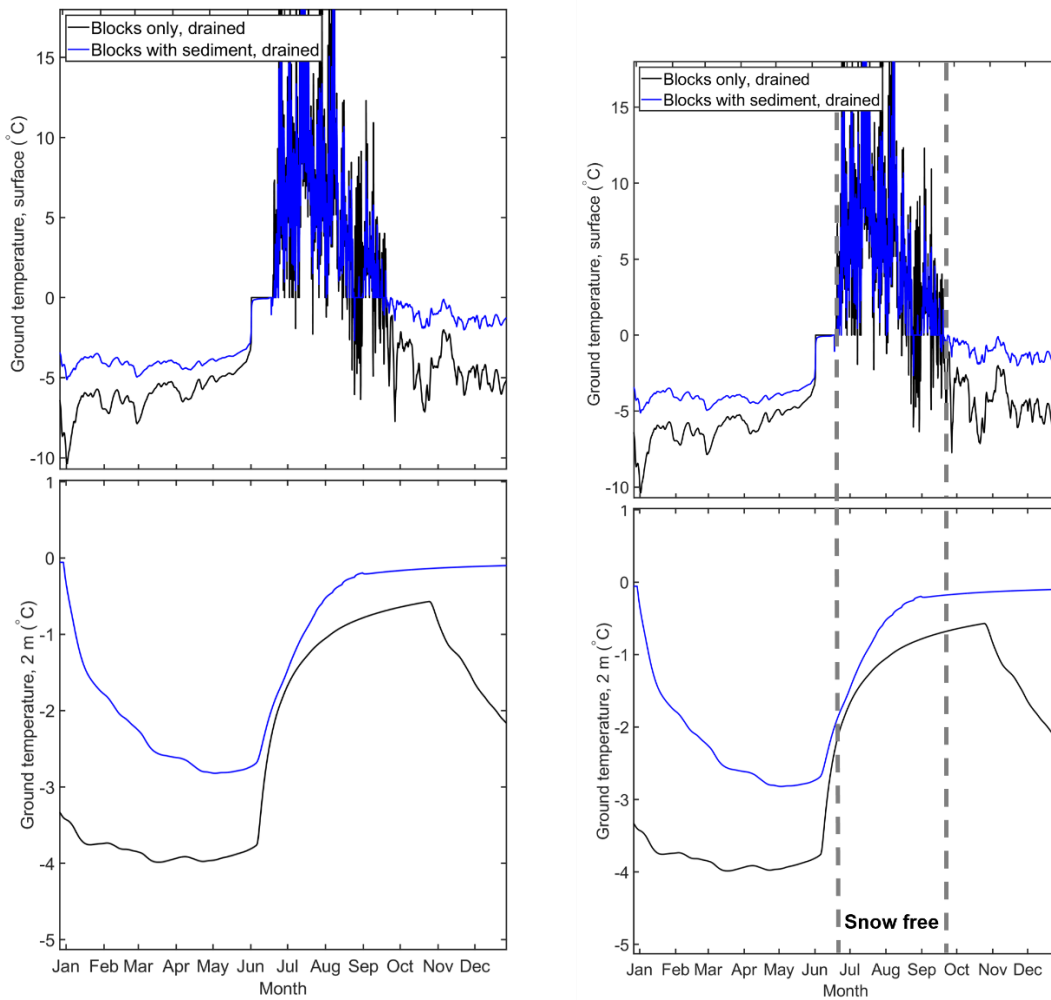


533

534 **Figure 45: Equilibrium ground temperature at 2 m depth for three idealized stratigraphies (Table 1) and different snowfall factors.**
535 **Each data point represents one model run of one of the six scenarios at a certain snowfall factor.**

536 Annual maximum snow depths at a snowfall factor of 1.0 are between 1.5 m and 2.4 m at Juvvasshøe and between
537 0.4 m and 1.0 m at Ivarsfjorden. At Juvvasshøe, all three *undrained* scenarios feature positive ground temperatures at snowfall
538 factors of 0.75 and above, which corresponds to permafrost-free conditions. Temperatures in the *blocks with sediment, drained*
539 and *sediment only, drained* runs are positive for a snowfall factor of 1.0 and above. The ground temperature in the *blocks only,*
540 *drained* runs remains below -1.0 °C for all snowfall scenarios. A similar pattern is seen in Ivarsfjorden, although a snowfall
541 factor of 1.5 results in positive temperatures for the scenario *blocks only, drained* which is clear evidence of the overall warmer
542 ground temperatures. Temperatures for the *blocks with sediment* stratigraphy are positive for snowfall factors exceeding 0.5,
543 and exceeding 0.75 for the other scenarios (with the exception of the *blocks only, drained* scenario, see above). For snowfall
544 factors above 0.25, ground temperature at 2 m depth increase with snow depth as a result of increased insulation-of the ground
545 during winter. However, the increase from a snowfall factor of 0 to 0.25 leads to a slight cooling for the *drained* scenarios as
546 opposed to a slight warming in the *undrained* scenarios. The reason for this cooling is likely the higher winter albedo of the
547 completely snow-free ground (for snowfall factor zero), which outweighs the insulating of the shallow snow cover for snowfall
548 factor 0.25.

549 Fig. 5 shows simulated temperatures for one year at the ground surface and 2 m depth for drained conditions for both
550 *blocks only* and the *blocks with sediment* scenarios for Juvvasshøe (snowfall factor 0.75). While ground surface temperatures
551 are largely similar during the snow-free summer season, they decrease much faster in fall for the *blocks only* compared to the
552 *blocks with sediment* scenario, wherefor which the slow refreezing of the active layer leads to a prolonged warming of the
553 ground surface from below. In the *blocks only* scenario, on the other hand, the active layer contains only little water, so that
554 refreezing occurs within only a short time period. The rapid cooling in the *blocks only* scenario is also visible within the
555 permafrost table at 2 m depth, resulting in lower winter temperatures compared to the *blocks with sediment* curve and thus
556 explaining the simulated differences in MAGT.

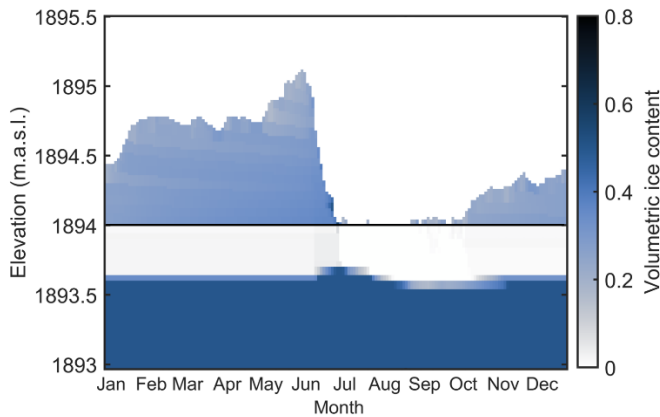


557

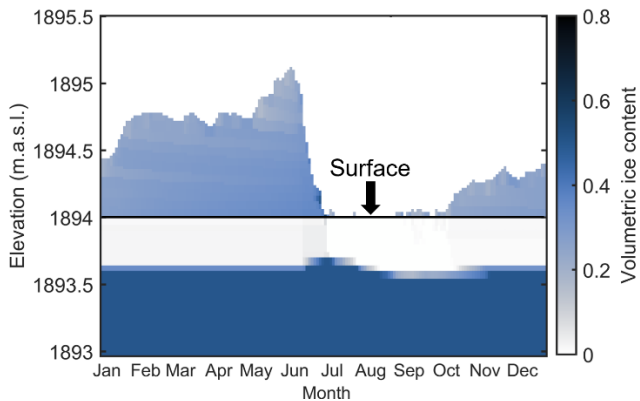
558 **Figure 56:** Modelled ground temperature at 0.05 m (top) and 2 m (bottom) depth for the *blocks only, drained* and *blocks with sediment,*
 559 *drained* scenarios during a year of an equilibrium run at Juvvashøe. *S_f = 0.75*, for *sf = 0.75*. The snow-free summer season is
 560 highlighted. Note that the upper plot is truncated at 17 °C, maximum summer temperatures are 26 °C in both scenarios.

561

562 FigureFig. 6 shows the corresponding snow cover and volumetric ground ice content in the upper meter of the ground
 563 for the *blocks only, drained* scenario. A largely stable ground ice table forms already at a depth of about 0.5 m, while the active
 564 layer is almost free of ground ice in winter, corresponding to the low water ~~content~~contents for thawed condition, enabling
 565 rapid refreezing and thus strong cooling during winter. During and after snow melt, meltwater infiltrates in the blocky layer
 566 and refreezes at the then very cold ice table, resulting in the formation of new ground ice which slowly melts during the course
 567 of summer. The slight increase of the ground ice table in early winter is due to refreezing of residual water above the ice table
 568 from rain and snow melt events in October which has not fully drained before refreezing.



569



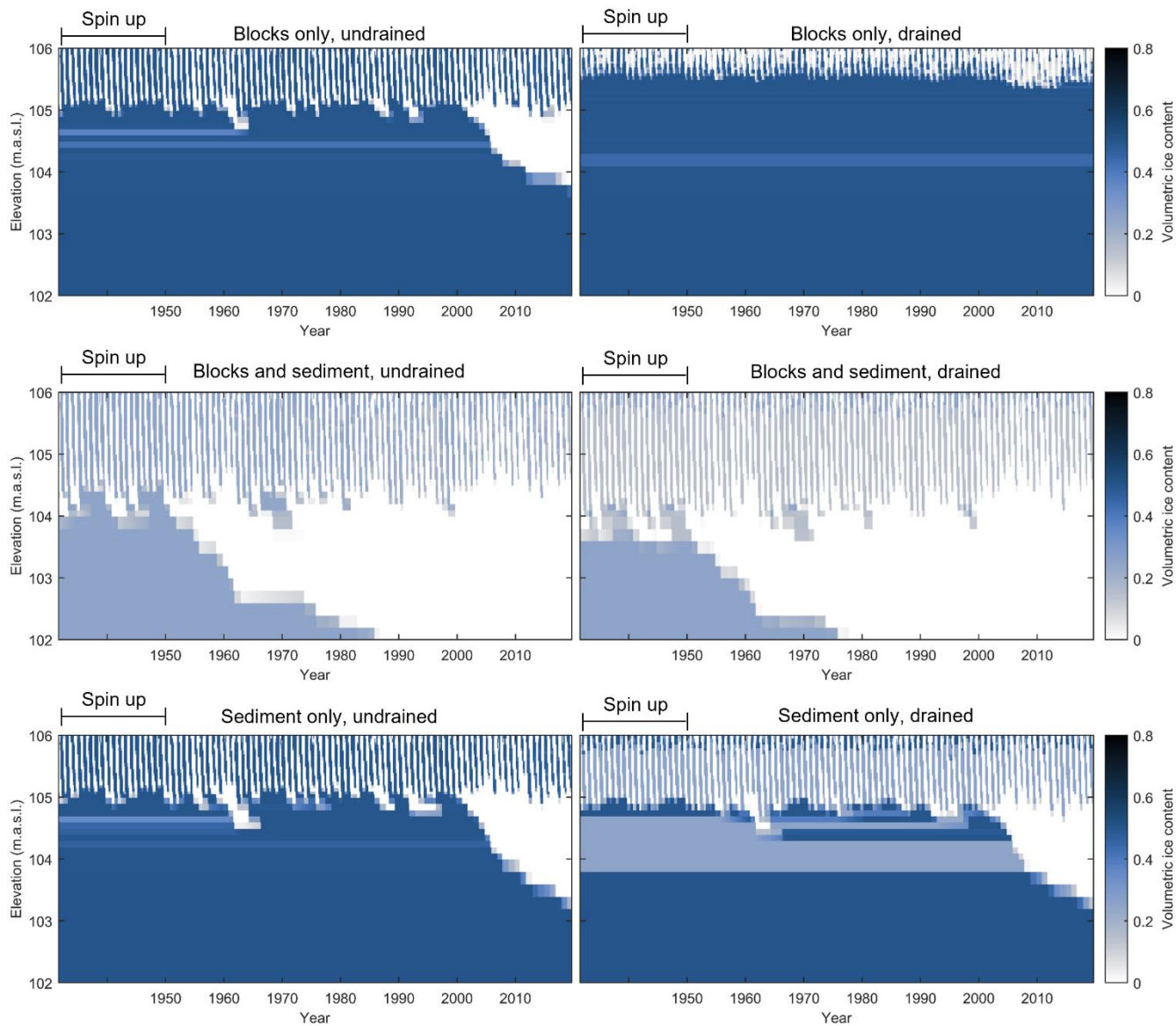
570

571 **Figure 67: Modelled volumetric ground ice content in the upper 1 m of the ground ($\le 1894\text{ m}$ (below 1894 m) and the snow cover**
 572 **($\ge 1894\text{ m}$ (above 1894 m) for the *blocks only, drained* scenario, during one year of an equilibrium run at Juvvasshøe, for $sf = 0.75$.**
 573 **Note the rise of the ground ice table in June after infiltrated snow melt water refreezes. $Sf = 0.75$.**

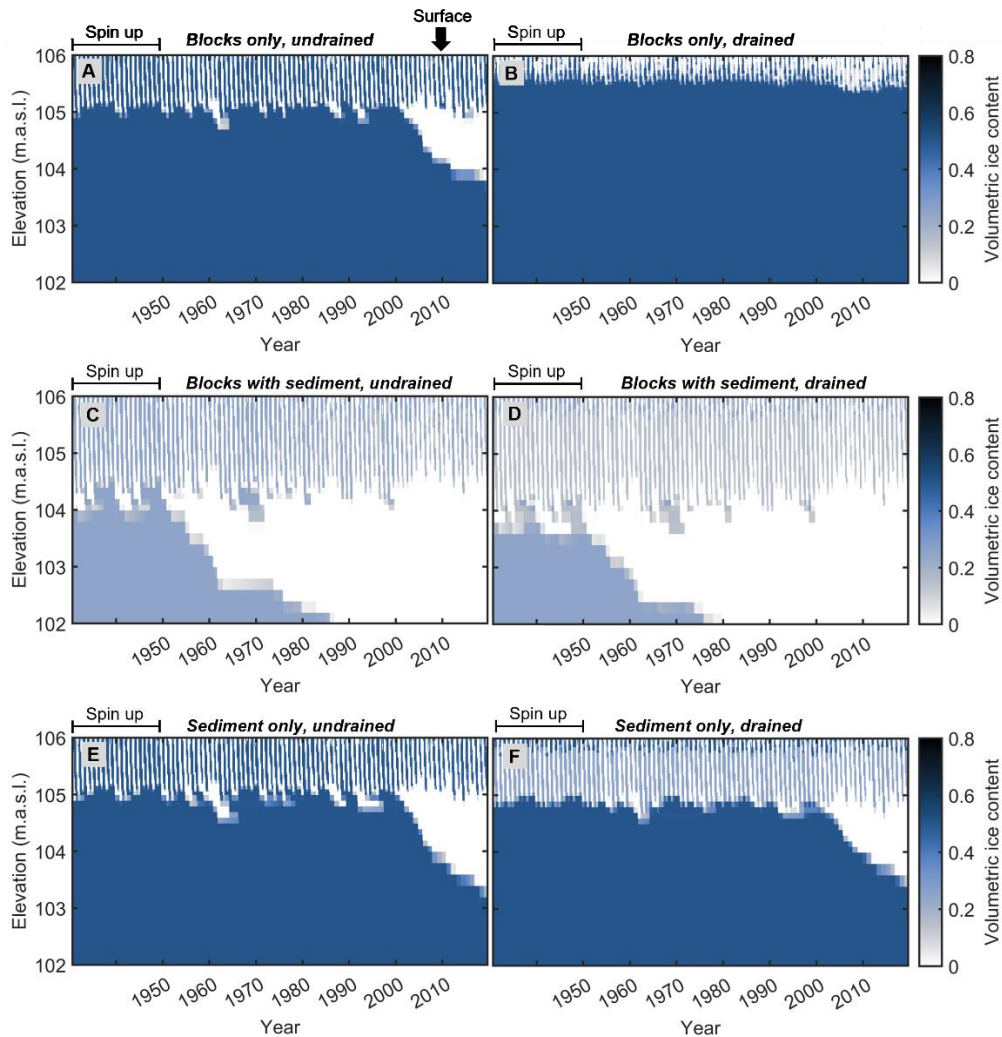
574 4.3 Transient response of ground temperatures and ice content to climate warming

575 The ERA5 reanalysis dataset allows us to model simulate the evolution of the ground thermal regime and ground ice content
 576 from 1951 to 2019. Figure, during which mean air temperatures increased from $-4.5\text{ }^{\circ}\text{C}$ (1951-1960) to $-3.8\text{ }^{\circ}\text{C}$ (2010-2019)
 577 for Juvvasshøe and from $0.5\text{ }^{\circ}\text{C}$ (1951-1960) to $1.2\text{ }^{\circ}\text{C}$ (2010-2019) at Ivarsfjorden. Fig. 7 shows the ground ice content for
 578 the different scenarios in Ivarsfjorden. In all simulations, a stable ice table and permafrost conditions form during the spin up
 579 period, (using model forcing for the cold period 1962-1971, Table 2), with volumetric ice contents of 0.5 (*blocks only, sediment*
 580 only) and -0.25 (*blocks with sediment*) according to the applied stratigraphy (table 1 Table 1). In the period 1951 to 2019,
 581 ground ice contents evolves content evolve as a response to the applied climate forcing, showing different responses of the
 582 ground ice table. In the *blocks only, drained* scenario, the ice table perennial ice table in the upper 5 m (so between the active
 583 layer and the bedrock) does not lower by a significant amount, (2 % lowering), while the ice table lowers significantly in all

584 ~~other simulations.~~by 33 % in the *blocks only, undrained scenario*. The ~~perennial~~ice table in the ~~upper 5 m of the~~*blocks with*
585 *sediment* stratigraphy ~~disappeared~~disappears by 1985 and 1975 in the *undrained* and *drained* scenarios, respectively. Finally,
586 the *sediment only* simulations show an intermediate effect where the ice table has ~~dropped to approximately half of its initial~~
587 ~~height by 2019.~~lowered by 41 % and 39 % for *undrained* and *drained* conditions respectively by 2019. The complete
588 ~~degradation in the blocks with sediment runs compared to partial degradation in all other scenarios (except blocks only, drained)~~
589 ~~is not unexpected since this stratigraphy has a 25% porosity (and thus ice content), compared to 50% in the others.~~ We conclude
590 that the ground stratigraphy and drainage conditions strongly control the response of the ground towards warming, with full
591 degradation near-surface permafrost in both *blocks with sediment* runs, partial degradation in the *blocks only, undrained* run
592 and in both *sediment only* runs and finally continued stable permafrost conditions in the *blocks only, drained* simulation. At
593 the Juvvasshøe site, the ice table ~~persists~~remain stable in all simulations, but a slight lowering occurs in the *blocks with*
594 *sediment* scenarios.



595



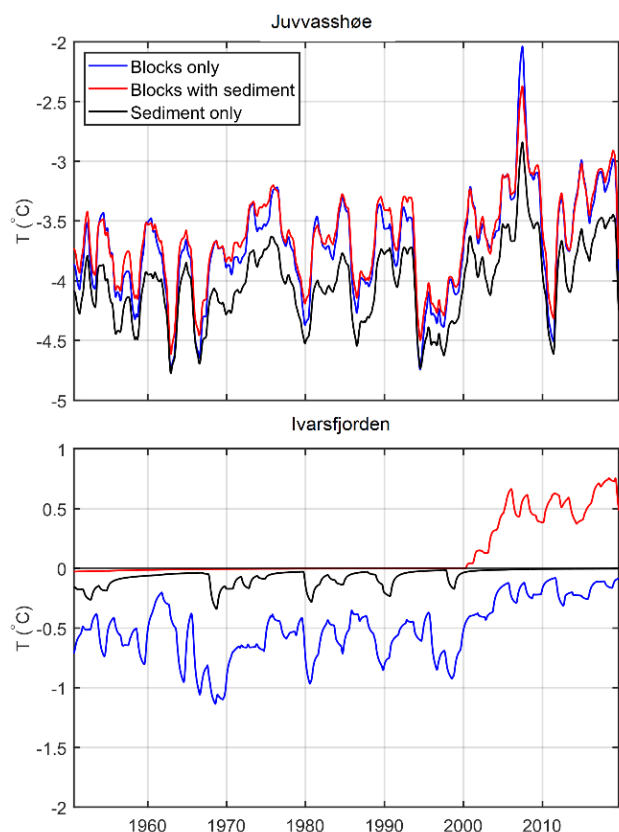
596

597 **Figure 78: Modelled volumetric ground ice content at Ivarsfjorden between 1951 and 2019 for the idealized stratigraphies in**
 598 **undrained and drained conditions. The and $sf = 1.0$ in all simulations.**

599 **The changes in ground temperature are also strongly dependent on surface elevation is at 106 m.a.s.l. In the stratigraphy,**
 600 **Figure active layer, ice contents increase and decrease annually, corresponding to the active layer refreezing and thawing.**

601 **Fig. 8** shows the change in temperatures at 5 m depth for the *drained* scenarios, which at the Ivarsfjorden rock glacier
 602 (snowfall factor 1.0) correspond to a full (*blocks with sediment*) and partial (*sediment only*) lowering of the ice table, as well
 603 as a relatively stable (*blocks only*) ice table. The *blocks only* simulation ~~underwent~~ shows an increase from $-0.6\text{ }^{\circ}\text{C}$ to $-0.2\text{ }^{\circ}\text{C}$
 604 between the 1951–1960 and 2010–2019 means, not being strongly influenced by latent heat effects due to the relative stable
 605 ice table. The *sediment only* case ~~experienced~~ experiences only minimal warming in this period at 5-m depth, as it is strongly
 606 influenced by the ongoing ground ice melt which confines ground temperatures to close to $0\text{ }^{\circ}\text{C}$. Finally, the complete

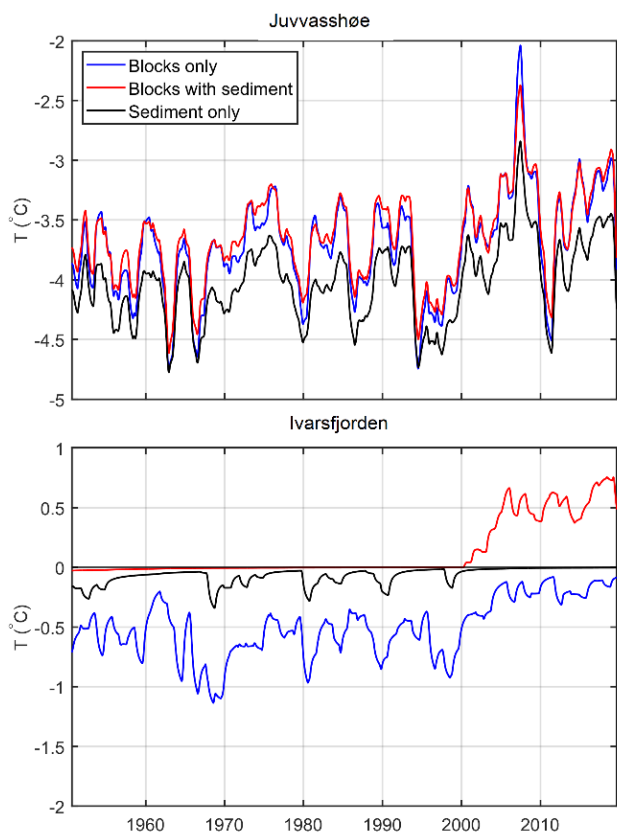
607 ~~degradation/disappearance of the ground ice table in blocks with sediment run coincided with in a warming to positive~~
 608 ~~temperatures, from 0.0 °C to 0.6 °C. Ground temperatures at 5 m depth were lower for snowfall factor 0.5 and resulted in less~~
 609 ~~ice melt, so that the warming between the 1951–1960 and 2010–2019 means were from -0.8 °C to -0.3 °C in the blocks only~~
 610 ~~stratigraphy, from -0.5 °C to 0.0 °C in the sediment only stratigraphy and from -0.1 °C to 0.1 °C in the blocks with sediment~~
 611 ~~stratigraphy.~~



612
 613 **Figure 8: Ground temperature at 5 m depth for the idealized stratigraphies under drained conditions. $sf = 1.0$ for Ivarsfjorden and**
 614 **$sf = 0.25$ for Juvvasshøe.**

615 At Juvvasshøe, permafrost degradation and thus strong ground ice melt does not occur for any of the scenarios for snowfall
 616 factor 0.25 (Fig. 8). Nevertheless, the warming rates differed to some degree between the scenarios. In the blocks only
 617 simulation, 5m, and ground temperatures only increased from -3.7 by 0.2 °C to -3.5 °C between the 1951–1960 and 2010–
 618 2019 means, from -3.8 °C to -3 (blocks only) to 0.4 °C for the (blocks with sediment run ranged and from -4.1 °C to -3.7 °C in
 619 the sediment only run. For snowfall factor 0.5, the change in temperature at 5 m depth in drained scenarios were overall higher,
 620 i.e. from -3.1 °C to -2.6 °C for the blocks only stratigraphy, from -2.5 °C to -1.9 °C for the blocks with sediment stratigraphy
 621 and from -2.9 °C to -2.4 °C for the sediment only stratigraphy. In conclusion, the warming rates appear more sensitive to

622 ~~changes in the amount) between the 1951–1960 and 2010–2019 means (Fig. 8). The results of snowfall than to differences in~~
623 ~~the transient runs indicate that the subsurface stratigraphy and drainage conditions, unless strongly affect the timing of~~
624 permafrost degradation ~~and thus strong in blocky terrain. While~~ ground ice melt ~~occur~~ controls the warming rates at
625 Ivassfjorden, only small differences in warming rates are simulated for the still stable permafrost in Juvasshøe. However, we
626 emphasize that the simulations at Juvasshøe were performed for a shallow snow cover ($sf = 0.25$) for which is accompanied
627 by low rates of warming—differences in modeled ground temperatures are small (Fig. 5).



628

629 Figure 9: Ground temperature at 5 m depth for the idealized stratigraphies under drained conditions; $sf = 1.0$ for Ivassfjorden and
630 $sf = 0.25$ for Juvasshøe.

631 5. Discussion

632 5.1 Limitations of the model setup

633 In this study, CryoGrid has been applied at two permafrost sites in Norwegian mountain environments. At both sites, we set
634 up validation runs to benchmark the performance of model system against measurements of ground (Juvasshøe) and ground
635 surface (Ivassfjorden) temperatures. At Juvasshøe, the model can largely reproduce the annual cycle of measured ground

636 temperatures at the PACE borehole, when the snowfall is reduced to account for the generally shallow snow cover at the site.
637 At Ivarsfjorden, ~~the~~ simulations with full snowfall yielded a similar performance for the *blocks only*, *drained scenario* ground
638 surface temperature, approximately reproducing the mean of measurements at 11 sites. A statistical evaluation at both sites
639 indicated a cold bias of the model of approximately -0.5 °C which we considered acceptable, considering the spatial variability
640 of the ground thermal regime at both sites (see Gisnås et al. 2014 for Juvasshøe). At Ivarsfjorden, the transient simulations are
641 in broad agreement with observations at the rock glacier which indicate that permafrost ~~is or~~ has been present in the recent
642 past (Lilleøren et al., 2022). ~~This is remarkable as the site is located far outside the mapped permafrost range (e.g. Gisnås et~~
643 ~~al., 2017), which is corroborated by the other scenarios (representing “normal” ground) in~~ Permafrost conditions are simulated
644 for all stratigraphies during model spin using the cold period 1962-1971 for which near surface permafrost no longer exists.
645 Modelled MAGSTs fall within the 25th and 75th percentile of measured MAGSTs between July 2016 and July 2019. However,
646 modelled MAGSTs are colder than the mean and median measurements, indicating a small potential bias of the model of
647 approximately -0.5 °C, temperatures are closest to Little Ice Age conditions when the rock glacier was likely active.

648 Within the model setup, in particular the exact ground stratigraphy and other poorly constrained parameters, such as
649 the albedo, give rise to uncertainties ~~when comparing to measurements.~~ While the real porosity of the ground is unknown,
650 sensitivity tests show a maximum of 0.4 °C differences in simulated ground temperatures between the highest and lowest
651 porosity values tested (Supplement). Only at Juvasshøe, the stratigraphy has been described from the borehole (Isaksen et al.,
652 2003), while no thorough evaluation of the subsurface stratigraphy is available for Ivarsfjorden. Lilleøren et al. (2022)
653 described the site as a complex creeping system with inhomogeneous subsurface properties. Most of the rock glacier surface
654 is described as ‘relict’ (Lilleøren et al., 2022) with sand and gravel in between blocks. For these ‘relict’ areas, the simulations
655 for the *blocks with sediment* ~~and *sediment only*~~ stratigraphy, in which near-surface permafrost fully or partially degrades, could
656 indeed represent the thermal state adequately. This is supported by the validation run with the *blocks with sediment* stratigraphy
657 which yielded a good fit with ground surface temperature measurements at sites largely located on this ‘relict’ surface
658 (Lilleøren et al., 2022). Two areas are described as ‘fresh’ which could indicate lateral movements due to the presence of
659 ground ice. These contain larger blocks and could thus be better described by the *blocks only* stratigraphy for which permafrost
660 and ground ice still persist at the end of the simulations. However, also in these ‘fresh’ areas, the amount of finer sediment is
661 unclear, in particular in deeper layers. In our simulations, we have only considered a single, homogeneous layer in the
662 uppermost 5 m in order to compare the thermal regime and ground ice dynamics for idealized stratigraphies. In reality, ground
663 stratigraphies in blocky terrain can feature aspects of all scenarios, for example a blocky layer with air-filled voids on top,
664 followed by blocks filled with sediments and a sediment only layer in the bottom. For the cooling effect described in this study,
665 it is critical that the blocky top layer is deep enough so that a ground ice table from which water can drain can form within.
666 Therefore, it is likely that also shallower blocky layers with air-filled voids can lead to lower ground temperatures, depending
667 on the climatic conditions which determine the depth of the ground ice table.

668 We emphasize that a consistent model setup was selected for all scenarios, so that uncertainties caused by other parts
669 of the model system influence them all in a similar, consistent way. In particular, none of the convective processes summarized

670 by Harris and Pedersen (1998) that cause a negative thermal anomaly in blocky terrain are considered in the model setup. The
671 same applies to the effect of rocks protruding into and through the snow cover as was described by Juliussen and Humlum
672 (2008) which could potentially be included in CryoGrid by laterally coupled simulations (e.g. Zweigel et al. 2021) with snow
673 redistribution between tiles representing blocks of different heights. Considering air convection in future simulations (as e.g.
674 in Wicky and Hauck, 2017) should become a priority for model development as this is likely to interact with the ground ice
675 mass balance for the blocky drained scenario and could thus exacerbate the thermal anomaly.

676 Further uncertainties are related to the model forcing data. The ERA5 reanalysis data is a global product with coarse
677 horizontal resolution, so that the TopoSCALE downscaling routine (Fiddes and Gruber 2014) is applied to obtain more
678 representative meteorological forcing. Nonetheless, as mentioned in Fiddes and Gruber (2014) ~~as well as Fiddes et al. (2019)~~
679 and Fiddes et al. (2019; 2022), there are ~~also some~~ limitations to this scheme, in particular the primitive downscaling scheme
680 for precipitation, which only interpolates between ERA5 grid points and thus misses the effects of local orography. The same
681 is true for the effects of local cloud build-up around slopes and mountains, which affects the radiation budget. While these
682 uncertainties could affect the comparison of model results to field measurements (Sect. 4.1), the model forcing data can
683 certainly capture the regional-scale climate characteristics of the two study sites, e.g. the significant differences in MAAT
684 between the two sites. The thermal anomaly of the *blocks only, drained* scenario consistently occurs for both sites and thus
685 over a significant range of climate conditions, so that the effect is likely robust despite the uncertainties in the model forcing
686 data. The same is true for the uncertainty caused by the Crocus-based snow scheme (Vionnet et al. 2012; Zweigel et al., 2021).
687 In this study, we have performed a sensitivity study with respect to the amount of snow (by modifying the snowfall factor,
688 Sect. 4.2), but simply scaling snowfall cannot represent the true time evolution of the snow cover due to wind redistribution
689 (e.g. Liston & Sturm, 1998; Martin et al., 2019). possibly resulting in differences between observed and simulated
690 temperatures. Nevertheless, it seems unlikely that the exact time dynamics of snow ablation and/or deposition events strongly
691 affects the dependence of the thermal anomaly in the *blocks only, drained* -scenario on overall winter snow depths. We
692 therefore conclude that the significant negative thermal anomaly for the blocks only, drained scenario is likely robust in the
693 light of the model uncertainty.

694 5.2 The effect of the ground ice dynamics on ground temperatures

695 Despite the uncertainties of the model setup, our results show a clear negative thermal anomaly for the *blocks only, drained*
696 scenario. If the winter snow depth is sufficiently high, a surface cover of coarse blocks with air-filled voids (i.e. high porosity
697 and low water holding capacity) results in 2 m ground temperatures 1 to 2 °C lower than for the other stratigraphies. In the
698 Ivarsfjorden simulations, the *blocks only, drained* scenario is the only one where near-surface permafrost conditions persist
699 even today, while near-surface permafrost degrades for the *blocks with sediment* and *sediment only* scenarios. This is
700 accompanied by a strong thermal offset, with a MAGST mean ground surface temperature of more than 2 °C for the *blocks*
701 *only, drained* scenario, while MAGT the mean ground temperatures at 2 m were below 0 °C. Interestingly, the temperature
702 anomaly appears largely constant over time in the transient simulations, except for periods when permafrost disappears in one

703 of the scenarios and confines ground temperatures to 0 °C, which delays further ground warming. For lower snow depths, the
704 temperature anomaly becomes smaller and eventually vanishes for the (~~generally~~largely irrelevant) case of permanently snow-
705 free conditions.

706 The negative temperature anomaly largely accumulates during fall and winter (Fig. 5). ~~As the~~6. The active layer
707 contains very little water in the *blocks only, drained* scenario, ~~it rapidly refreezes~~. Dry soils have a lower thermal conductivity
708 compared to wet soils, but the lack of latent heat release allows for rapid refreezing during fall which enables a fast cooling of
709 the deeper soil layers and thus leads to overall lower winter temperatures. In spring, this “cold content” (i.e. sensible heat) of
710 the ground is partly transformed into the build-up of new ground ice (i.e. latent heat, Fig. 6) which only melts slowly during
711 summer due to the insulation of the overlying blocky layer. This timing of the ground ice formation is strongly different from
712 all other scenarios, for which ground ice mostly forms in fall/early winter due to refreezing of the water contained in the active
713 layer (e.g. Hinkel et al., 2001). A somewhat similar effect has been described for peat plateaus in northern Norway where
714 simulations yielded 2 °C lower temperatures for well-drained peat compared to water-saturated peat (Martin et al., 2019). This
715 refreezing of the active layer can take several months and is further delayed if a significant snow cover forms during this
716 period, which leads to overall higher winter temperatures in the permafrost- due to the insulation (Zhang, 2005). It is exactly
717 for these “high-snow situations” (corresponding to higher snowfall factors in our sensitivity analyses) that the temperature
718 anomaly of the *blocks only, drained* scenario is largest. Our results for example suggest that permafrost can occur for blocky
719 ground on slopes around Juvvasshøe, even if the winter snow cover exceeds 2 m thickness.

720 We note that the thermal anomaly caused by the ground ice dynamics in blocky ground is not related to convective
721 processes (Harris and Pedersen, 1998) or the effect of blocks protruding through the snow cover (Juliussen and Humlum, 2008;
722 Gruber Hoelzle, 2008). ~~A somewhat similar effect has been described for peat plateaus in northern Norway where simulations~~
723 ~~yielded 2 °C lower temperatures for well drained peat compared to water saturated peat (Martin et al., 2019)~~. The simulated
724 temperature anomaly is similar to the 1.3–2.0 °C lower temperatures that Juliussen and Humlum (2008) found in blockfields
725 compared to till and bedrock in Central-eastern Norway. While a complete process model for blocky ground and rock glaciers
726 will certainly have to take air convection and the interplay between surface blocks and the snow cover into account, it is
727 encouraging- that the relatively simple model approach presented in this work offers prospects to improve our estimates of
728 permafrost occurrence in mountain environments.

729 In a first-order approach, thermal anomalies can be translated into elevation differences by assuming a temperature
730 lapse rate, so that the impacts on the lower altitudinal limit of permafrost can be estimated. For a lapse rate of 0.5 °C per 100
731 m (e.g. Farbrot et al., 2011), the lower limit of permafrost in drained, blocky deposits in Norway would be 300 to 400 m lower
732 compared to “normal” permafrost represented by the other scenarios. For the Ivarsfjorden site, these numbers compare
733 favorably to the Scandinavian permafrost map (Gisnås et al., 2017) which shows a lower discontinuous permafrost limit in
734 Finnmark at around 400 m a.s.l., ~~approx~~-approximately 300 m above the rock glacier.

735 5.3 Implications for future work

736 In this study, we show that modelling the full subsurface water and ice balance in well-drained blocky deposits with air-filled
737 voids leads to significantly lower ground temperatures in permafrost environments. In modelling studies on the distribution of
738 permafrost, blocky ground usually is not accounted for, or the water balance is not simulated at this level of detail. For the
739 Northern hemisphere permafrost map (Obu et al., 2019), a coarse landcover classification was used in mountain areas which
740 did not represent blocky terrain. To produce the map, a semi-empirical equilibrium TTOP model was used in which the thermal
741 anomaly of blocky deposits likely could account for by adjusting the r_k parameter which accounts for the thermal offset of the
742 ground. A more sophisticated modelling approach as presented in this work could be used to train the more simple TTOP
743 model across a range of climate conditions. Permafrost mapping with transient models (e.g. Jafarov et al., 2012) often uses
744 fixed ground stratigraphies, in which the sum of water and ice contents does not change for a given layer. An example is the
745 transient permafrost map for southern Norway (Westermann et al., 2013) which featured a dedicated stratigraphic class for
746 blocky deposits, with a dry upper layer followed by an ice-saturated layer below, very similar to the stratigraphy used for the
747 *blocks only, drained* scenario in this study. However, both layers have a fixed thickness and the sum of water and ice contents
748 is constant, so that the temporal evolution of ground ice dynamics cannot be captured. If the seasonal thaw extends in the ice-
749 rich layer, a pool of meltwater forms which cannot drain and hence strongly delays refreezing in fall, potentially resulting in
750 the degradation of permafrost. In our simulations with full water/ice dynamics, the ice table instead varies over time, both
751 seasonally and over longer periods in response to the climatic forcing. Such changes in the ground ice table have for example
752 been observed at the Schilthorn site in the European Alps where the ground ice table was significantly lowered during a hot
753 summer and did not regrow in the following years although permafrost conditions persisted (Hilbich et al., 2008). As ~~the~~this
754 observation site is located on a slope, it is clear that such observed ground ice dynamics can only be reproduced if lateral
755 drainage of meltwater is taken into account. To improve transient modelling of mountain permafrost distribution, CryoGrid in
756 the configuration used in this study could be adapted for individual grid cells, especially by adjusting the strength of the lateral
757 drainage (i.e. the distance to seepage face) depending on the local slope. In flat areas and depressions, water would then pool
758 up as for the *undrained* cases, while both melt- and rainwater would drain in sloping terrain as in the *undrained* cases, with
759 corresponding changes to the ground thermal regime and permafrost distribution. Furthermore, our study suggests that the
760 presence of fine sediments in the voids between blocks can strongly alter the ground temperature compared to blocky terrain
761 with air-filled voids. For spatially distributed mapping, these two cases would have to be distinguished as separate stratigraphic
762 classes and maps of their spatial extent must be available. Especially the latter is expected to be significant challenge, as the
763 surfaces likely appear similar for remote sensors, so that detailed field mapping may be required.

764 The model approach in this study also offers significant potential to study ground ice derived runoff from blocky
765 deposits and rock glaciers. While the Norwegian study sites are both located in wet climate settings with ample water supply,
766 rock glaciers in more arid regions can be important sources of water (e.g. Croce and Milana 2002). The global ratio of rock
767 glacier to glacier water volume equivalent (WVEQ) is currently increasing as both systems react differently to a changing

768 climate –(Jones et al., 2019). Therefore, simulations of ground ice volumes and seasonal runoff characteristics in both the
769 present and future climates can be a valuable tool for the assessment of water resources. Furthermore, rock glaciers are sensitive
770 to climate change (Haeberli et al., 2010) and recent studies have linked rock glacier acceleration to increasing air temperatures
771 (e.g. Käab et al., 2007; Hartl et al., 2016; Eriksen et al., 2018). Our model approach is likely able to simulate the seasonal
772 ground ice mass balance at different points and elevations of a rock glacier which could be ingested in a flow model for rock
773 glaciers (e.g. Monnier ~~an~~and Kinnard, 2016). Finally, permafrost degradation and ground ice loss can also play an important
774 role for slope stability in mountain permafrost environments (e.g. Gruber and Haeberli, 2007; Saemundsson et al. 2018; Nelson
775 et al., 2001). Simulations of ground ice table changes, as well as the occurrence of strong melt events with corresponding
776 production of meltwater, could eventually improve assessments of the stability and hazard potential of permafrost-underlain
777 slopes (e.g. Mamot et al., 2021).

778 6. Conclusions

779 In this study, we used the CryoGrid permafrost model to simulate the effect of blocky terrain on the ground thermal regime
780 and ground ice dynamics at two Norwegian mountain permafrost sites (Juvvasshøe and Ivarsfjorden rock glacier). ~~We used~~In
781 particular, we investigated the effect of subsurface drainage, as typical on slopes, for three idealized stratigraphies, named
782 blocks only, blocks with sediment and drainage conditions (referred to as ‘scenarios’) to investigate thermal anomalies for
783 different amounts of snowfall~~sediment only~~. From this study, the following conclusions can be drawn:

784

- 785 • Markedly lower ground temperatures are found in well drained, coarse blocky deposits with air-filled voids (~~denoted~~
786 *blocks only, drained* scenario) compared to other scenarios which are either undrained or feature fine sediments. ~~The~~
787 This negative thermal anomaly ~~is up to 1.8–2. can exceed 2 °C, with and is mainly linked to differences in the freeze-~~
788 thaw dynamics caused by the removal of meltwater and the build-up of new ground ice in spring. The largest
789 ~~values~~anomalies occur in simulations with a thick winter snow cover as ground temperatures in well drained blocky
790 deposits are less sensitive to insulation by snow than other soils. We emphasize that the model does not account for
791 well-known factors, such as air convection and the effect of blocks protruding through the winter snow cover. ~~The~~
792 ~~negative thermal anomaly is mainly linked to differences in the freeze thaw dynamics caused by the removal of~~
793 ~~meltwater and the build up of new ground ice in spring.~~
- 794 • For the *blocks only, drained* scenario, thermally stable permafrost can exist at the Ivarsfjorden rock glacier site
795 (located near sea level), even for a mean annual ground surface temperature (MAGST) of 2.0–2.5 °C. At Juvvasshøe
796 in the southern Norwegian mountains, permafrost is simulated even for a very thick winter snow cover in the *blocks*
797 *only, drained* scenario, while all other scenarios in this case feature permafrost-free conditions.
- 798 • Transient simulations since 1951 at the Ivarsfjorden rock glacier show a completely or partially degraded ground ice
799 table for all scenarios, except the *blocks only, drained* scenario. This result is explained by the overall lower ground

800 temperatures in this scenario, while the simulated warming rates are generally similar for all scenarios, except for
801 periods when strong ground ice melt occurs.

802

803 This study suggests that including subsurface water and ice dynamics can drive simulations of mountain permafrost dynamics
804 towards reality, which can for example improve estimates of the lower altitudinal limit of permafrost in blocky terrain. In
805 addition to permafrost distribution mapping, the presented model approach could be used to simulate the seasonal and multi-
806 annual evolution of the ground ice table, in addition to ground-ice derived runoff. It therefore represents a further step to a
807 better understanding and model representation of the permafrost processes in mountain environments.

808

809 *Code and data availability.* The CryoGrid source code and model setup files are available
810 <https://doi.org/10.5281/zenodo.6563651> (Renette, 2022). Field measurements at Juvvasshøe are from Etzelmüller et al. (2020).
811 Field measurements at Ivarsfjorden are from Lilleøren et al. (2022).

812

813 *Author contribution.* CR performed the model simulations, retrieved forcing data, wrote the draft manuscript and created all
814 figures. SW helped design the study, developed the model and provided ideas throughout the entire study. KA developed code
815 for retrieving and downscaling forcing data, assisted with this process and wrote text regarding the forcing data. KL and KI
816 provided field measurements, site descriptions and photos. RBZ and JA developed parts of the model. All authors contributed
817 with text and suggestions.

818

819 *Competing interests.* The authors declare that they have no conflict of interest.

820

821 *Acknowledgements.* This work was supported by ESA Permafrost_CCI (<https://climate.esa.int/en/projects/permafrost/>),
822 Permafrost4Life (Research Council of Norway, grant no. 301639), and Nunataryuk (EU grant agreement no. 773421), as well
823 as the Department of Geosciences, University of Oslo.

824

825 **References**

- 826 Aalstad, K., Westermann, S., Schuler, T. V., Boike, J., and Bertino, L.: Ensemble-based assimilation of fractional snow-
827 covered area satellite retrievals to estimate the snow distribution at Arctic sites, *The Cryosphere*, 12, 247–270,
828 <https://doi.org/10.5194/tc-12-247-2018>, 2018.
- 829 Arenson, L. U., Phillips, M., and Springman, S. M.: Geotechnical considerations and technical solutions for infrastructure in
830 mountain permafrost, in: *New permafrost and glacier research*, pp. 3–50, Nova Science Publishers, 2009.
- 831 Azócar, G. and Brenning, A.: Hydrological and geomorphological significance of rock glaciers in the dry Andes, Chile (27–
832 33 S), *Permafrost and Periglacial Processes*, 21, 42–53, <https://doi.org/10.1002/ppp.669>, 2010.
- 833 Croce, F. A. and Milana, J. P.: Internal structure and behaviour of a rock glacier in the arid Andes of Argentina, *Permafrost
834 and Periglacial Processes*, 13, 289–299, <https://doi.org/10.1002/ppp.431>, 2002.
- 835 Dahl, R.: Block fields, weathering pits and tor-like forms in the Narvik Mountains, Nordland, Norway, *Geografiska Annaler:
836 Series A, Physical Geography*, 48, 55–85, <https://doi.org/10.1080/04353676.1966.11879730>, 1966.
- 837 Eriksen, H., Rouyet, L., Lauknes, T., Berthling, I., Isaksen, K., Hindberg, H., Larsen, Y., and Corner, G.: Recent acceleration
838 of a rock glacier complex, Adjet, Norway, documented by 62 years of remote sensing observations, *Geophysical Research
839 Letters*, 45, 8314–8323, <https://doi.org/10.1029/2018GL077605>, 2018.
- 840 Etzelmüller, B., Berthling, I., and Sollid, J. L.: Aspects and concepts on the geomorphological significance of Holocene
841 permafrost in southern Norway, *Geomorphology*, 52, 87–104, [https://doi.org/10.1016/S0169-555X\(02\)00250-7](https://doi.org/10.1016/S0169-555X(02)00250-7), 2003.
- 842 Etzelmüller, B., Schuler, T. V., Isaksen, K., Christiansen, H. H., Farbrot, H., and Benestad, R.: Modeling the temperature
843 evolution of Svalbard permafrost during the 20th and 21st century, *The Cryosphere*, 5, 67–79, [https://doi.org/10.5194/tc-5-67-
2011](https://doi.org/10.5194/tc-5-67-
844 2011), 2011.
- 845 Etzelmüller, B., Guglielmin, M., Hauck, C., Hilbich, C., Hoelzle, M., Isaksen, K., Noetzli, J., Oliva, M., and Ramos, M.:
846 Twenty years of European mountain permafrost dynamics—the PACE legacy, *Environmental Research Letters*, 15, 104070,
847 <https://doi.org/10.1088/1748-9326/abae9d>, 2020.
- 848 Farbrot, H., Hipp, T. F., Etzelmüller, B., Isaksen, K., Ødegård, R. S., Schuler, T. V., and Humlum, O.: Air and ground
849 temperature variations observed along elevation and continentality gradients in Southern Norway, *Permafrost and Periglacial
850 Processes*, 22, 343–360, <https://doi.org/10.1002/ppp.733>, 2011.
- 851 Fiddes, J. and Gruber, S.: TopoSCALE v. 1.0: downscaling gridded climate data in complex terrain, *Geoscientific Model
852 Development*, 7, 387–405, <https://doi.org/10.5194/gmd-7-387-2014>, 2014.
- 853 Fiddes, J., Endrizzi, S., and Gruber, S.: Large-area land surface simulations in heterogeneous terrain driven by global data sets:
854 application to mountain permafrost, *The Cryosphere*, 9, 411–426, <https://doi.org/10.5194/tc-9-411-2015>, 2015.
- 855 Fiddes, J., Aalstad, K., and Westermann, S.: Hyper-resolution ensemble-based snow reanalysis in mountain regions using
856 clustering, *Hydrology and Earth System Sciences*, 23, 4717–4736, <https://doi.org/10.5194/hess-23-4717-2019>, 2019.

857 Fiddes, J., Aalstad, K., and Lehning, M.: TopoCLIM: rapid topography-based downscaling of regional climate model output
858 in complex terrain v1. 1, *Geoscientific Model Development*, 15, 1753–1768, <https://doi.org/10.5194/gmd-15-1753-2022>,
859 2022.

860 Gislén, K., Eitzinger, B., Lussana, C., Hjort, J., Sannel, A. B. K., Isaksen, K., Westermann, S., Kuhry, P., Christiansen, H.
861 H., Frampton, A., et al.: Permafrost map for Norway, Sweden and Finland, *Permafrost and periglacial processes*, 28, 359–378,
862 <https://doi.org/10.1002/ppp.1922>, 2017.

863 Gislén, K., ~~S.~~ Westermann, ~~S.~~ T. V. Schuler, T. ~~V.~~ Melvold ~~Litherland~~, K., ~~Isaksen, J. Boike~~, and ~~B.~~ Eitzinger, ~~B.~~ Small.:
864 A statistical approach to represent small-scale variation/variability of snow in a regional permafrost model/temperatures due to
865 snow cover, *The Cryosphere*, 8.6, pp. 2063–2074. <https://doi.org/10.1201-1215>, <https://doi.org/10.5194/tc-10-1201-2016>,
866 <https://doi.org/10.5194/tc-8-2063-2014>, 2014.

867 Gislén, K., Westermann, S., Schuler, T. V., Melvold, K., and Eitzinger, B.: Small-scale variation of snow in a regional
868 permafrost model. *The Cryosphere*, 10, 1201–1215, <https://doi.org/10.5194/tc-10-1201-2016>, 2016.

869 Göckede, M., Kittler, F., Kwon, M. J., Burjack, I., Heimann, M., Kolle, O., et al.: Shifted energy fluxes, increased Bowen
870 ratios, and reduced thaw depths linked with drainage-induced changes in permafrost ecosystem structure. *The Cryosphere*,
871 11(6), 2975–2996. <https://doi.org/10.5194/tc-11-2975-2017>, 2017.

872 Goodrich, L. E.: The influence of snow cover on the ground thermal regime. *Can. Geotech. J.*, 19, 421–432,
873 <https://doi.org/10.1139/t82-047>, 1982.

874 Gruber, S. and Haeberli, W.: Permafrost in steep bedrock slopes and its temperature-related destabilization following climate
875 change, *Journal of Geophysical Research: Earth Surface*, 112, <https://doi.org/10.1029/2006JF000547>, 2007.

876 Gruber, S. and Hoelze, M.: The cooling effect of coarse blocks revisited: a modeling study of a purely conductive mechanism,
877 Zurich Open Repository and Archive, 2008.

878 Haeberli, W., Hallet, B., Arenson, L., Elcinin, R., Humlum, O., Käab, A., Kaufmann, V., Ladanyi, B., Matsuoka, N.,
879 Springman, S., et al.: Permafrost creep and rock glacier dynamics, *Permafrost and periglacial processes*, 17, 189–214,
880 <https://doi.org/10.1002/ppp.561>, 2006.

881 Hanson, S. and Hoelze, M.: The thermal regime of the active layer at the Murtèl rock glacier based on data from 2002,
882 *Permafrost and Periglacial Processes*, 15, 273–282, <https://doi.org/10.1002/ppp.499>, 2004.

883 Harris, C., Haeberli, W., Vonder Mühl, D., and King, L.: Permafrost monitoring in the high mountains of Europe: the PACE
884 project in its global context, *Permafrost and periglacial processes*, 12, 3–11, <https://doi.org/10.1002/ppp.377>, 2001.

885 Harris, C., Arenson, L. U., Christiansen, H. H., Eitzinger, B., Frauenfelder, R., Gruber, S., Haeberli, W., Hauck, C., Hoelze,
886 M., Humlum, O., et al.: Permafrost and climate in Europe: Monitoring and modelling thermal, geomorphological and
887 geotechnical responses, *EarthScience Reviews*, 92, 117–171, <https://doi.org/10.1016/j.earscirev.2008.12.002>, 2009.

888 Harris, S. A. and Pedersen, D. E.: Thermal regimes beneath coarse blocky materials, *Permafrost and periglacial processes*, 9,
889 107–120, [https://doi.org/10.1002/\(SICI\)1099-1530\(199804/06\)9:2<107::AID-PPP277>3.0.CO;2-G](https://doi.org/10.1002/(SICI)1099-1530(199804/06)9:2<107::AID-PPP277>3.0.CO;2-G), 1998.

890 Hartl, L., Fischer, A., Stocker-waldhuber, M., and Abermann, J.: Recent speed-up of an alpine rock glacier: an updated
891 chronology of the kinematics of outer hochebenkar rock glacier based on geodetic measurements, *Geografiska Annaler: Series*
892 *A, Physical Geography*, 98, 129–141, <https://doi.org/10.1111/geoa.12127>, 2016.

893 Hersbach, H., Bell, B., Berrisford, P., Hirahara, S., Horányi, A., Muñoz-Sabater, J., Nicolas, J., Peubey, C., Radu, R., Schepers,
894 D., et al.: The ERA5 global reanalysis, *Quarterly Journal of the Royal Meteorological Society*, 146, 1999–2049,
895 <https://doi.org/10.1002/qj.3803>, 2020.

896 Hilbich, C., Hauck, C., Hoelzle, M., Scherler, M., Schudel, L., Völksch, I., Vonder Mühll, D., and Mäusbacher, R.: Monitoring
897 mountain permafrost evolution using electrical resistivity tomography: A 7-year study of seasonal, annual, and long-term
898 variations at Schilthorn, Swiss Alps, *Journal of Geophysical Research: Earth Surface*, 113,
899 <https://doi.org/10.1029/2007JF000799>, 2008.

900 [Hinkel, K. M. and Outcalt, S. I.: Identification of heat transfer processes during soil cooling, freezing, and thaw in central](#)
901 [Alaska, *Permafrost Periglac.*, 5, 217–235, <https://doi.org/10.1002/ppp.3430050403>, 1994.](#)

902 [Hinkel, K. M., Paetzold, F., Nelson, F. E., and Bockheim, J. G.: Patterns of soil temperature and moisture in the active layer](#)
903 [and upper permafrost at Barrow, Alaska: 1993–1999, *Global Planet. Change*, 29, 293–309, 2001.](#)

904 Hipp, T., Etzelmüller, B., Farbrot, H., Schuler, T., and Westermann, S.: Modelling borehole temperatures in Southern Norway–
905 insights into permafrost dynamics during the 20th and 21st century, *The Cryosphere*, 6, 553–571, [https://doi.org/10.5194/tc-](https://doi.org/10.5194/tc-6-553-2012)
906 [6-553-2012](https://doi.org/10.5194/tc-6-553-2012), 2012.

907 Humlum, O.: Active layer thermal regime at three rock glaciers in Greenland, *Permafrost and Periglacial Processes*, 8, 383–
908 408, [https://doi.org/10.1002/\(SICI\)1099-1530\(199710/12\)8:4<383::AID-PPP265>3.0.CO;2-V](https://doi.org/10.1002/(SICI)1099-1530(199710/12)8:4<383::AID-PPP265>3.0.CO;2-V), 1997.

909 Isaksen, K., Holmlund, P., Sollid, J. L., and Harris, C.: Three deep alpine-permafrost boreholes in Svalbard and Scandinavia,
910 *Permafrost and Periglacial Processes*, 12, 13–25, <https://doi.org/10.1002/ppp.380>, 2001.

911 Isaksen, K., Heggem, E., Bakkehøi, S., Ødegård, R., Eiken, T., Etzelmüller, B., and Sollid, J.: Mountain permafrost and energy
912 balance on Juvvasshøe, southern Norway, in: 8th International Conference on Permafrost, Zurich, Switzerland, ISI:
913 000185049300083, pp. 467–472, 2003.

914 Isaksen, K., Sollid, J. L., Holmlund, P., and Harris, C.: Recent warming of mountain permafrost in Svalbard and Scandinavia,
915 *Journal of Geophysical Research: Earth Surface*, 112, <https://doi.org/10.1029/2006JF000522>, 2007.

916 Jafarov, E. E., Marchenko, S. S., and Romanovsky, V.: Numerical modeling of permafrost dynamics in Alaska using a high
917 spatial resolution dataset, *The Cryosphere*, 6, 613–624, <https://doi.org/10.5194/tc-6-613-2012>, 2012.

918 Jones, D. B., Harrison, S., Anderson, K., and Whalley, W. B.: Rock glaciers and mountain hydrology: A review, *Earth-Science*
919 *Reviews*, 193, 66–90, <https://doi.org/10.1016/j.earscirev.2019.04.001>, 2019.

920 Juliussen, H. and Humlum, O.: Thermal regime of openwork block fields on the mountains Elgåhogna and Sølen, central-
921 eastern Norway, *Permafrost and Periglacial Processes*, 19, 1–18, <https://doi.org/10.1002/ppp.607>, 2008.

922 Kääb, A., Frauenfelder, R., and Roer, I.: On the response of rockglacier creep to surface temperature increase, *Global and*
923 *Planetary Change*, 56, 172–187, <https://doi.org/10.1016/j.gloplacha.2006.07.005>, 2007.

924 Langer, M., Westermann, S., Boike, J., Kirillin, G., Grosse, G., Peng, S., and Krinner, G.: Rapid degradation of permafrost
925 underneath waterbodies in tundra landscapes—toward a representation of thermokarst in land surface models, *Journal of*
926 *Geophysical Research: Earth Surface*, 121, 2446–2470, <https://doi.org/10.1002/2016JF003956>, 2016.

927 Liestøl, O.: Lokalt omrøde med permafrost i Gudbrandsdalen, *Norsk Polarinstitutt Aarbok*, 1965, 129–133, 1966.

928 [Liljedahl, A. K., Hinzman, L. D., Harazono, Y., Zona, D., Tweedie, C. E., Hollister, R. D., et al.: Nonlinear controls on](#)
929 [evapotranspiration in Arctic coastal wetlands. *Biogeosciences*, 8\(11\), 3375–3389. <https://doi.org/10.5194/bg-8-3375-2011>,](#)
930 [2011.](#)

931 Lilleøren, K. S. and Etzelmüller, B.: A regional inventory of rock glaciers and ice-cored moraines in Norway, *Geografiska*
932 *Annaler: Series A, Physical Geography*, 93, 175–191, <https://doi.org/10.1111/j.1468-0459.2011.00430.x>, 2011.

933 Lilleøren, K. S., Etzelmüller, B., Rouyet, L., Eiken, T., and Hilbich, C.: Transitional rock glaciers at sea-level in Northern
934 Norway, *Earth Surface Dynamics Discussions*, pp. 1–29, <https://doi.org/10.5194/esurf-2022-6>, 2022.

935 Liston, G. E. and Sturm, M.: A snow-transport model for complex terrain, *Journal of Glaciology*, 44, 498–516,
936 <https://doi.org/10.3189/S0022143000002021>, 1998.

937 [Luetsch, M., Stoeckli, V., Lehning, M., Haeberli, W., and Ammann, W.: Temperatures in two boreholes at Flüela Pass,](#)
938 [Eastern Swiss Alps: the effect of snow redistribution on permafrost distribution patterns in high mountain areas, *Permafrost*](#)
939 [Periglac., 15, 283–297. doi:10.1002/ppp.500, 2004.](#)

940 Mamot, P., Weber, S., Eppinger, S., and Krautblatter, M.: A temperature-dependent mechanical model to assess the stability
941 of degrading permafrost rock slopes, *Earth Surface Dynamics*, 9, 1125–1151, <https://doi.org/10.5194/esurf-9-1125-2021>,
942 2021.

943 Martin, L. C. P., Nitzbon, J., Aas, K. S., Etzelmüller, B., Kristiansen, H., and Westermann, S.: Stability conditions of peat
944 plateaus and palsas in northern Norway, *Journal of Geophysical Research: Earth Surface*, 124, 705–719,
945 <https://doi.org/10.1029/2018JF004945>, 2019.

946 Monnier, S. and Kinnard, C.: Interrogating the time and processes of development of the Las Liebres rock glacier, central
947 Chilean Andes, using a numerical flow model, *Earth Surface Processes and Landforms*, 41, 1884–1893,
948 <https://doi.org/10.1002/esp.3956>, 2016.

949 Nelson, F. E., Anisimov, O. A., and Shiklomanov, N. I.: Subsidence risk from thawing permafrost, *Nature*, 410, 889–890,
950 <https://doi.org/10.1038/35073746>, 2001.

951 Nesje, A., Matthews, J. A., Linge, H., Bredal, M., Wilson, P., and Winkler, S.: New evidence for active talus-foot rock glaciers
952 at Øyberget, southern Norway, and their development during the Holocene, *The Holocene*, 31, 1786–1796,
953 <https://doi.org/10.1177/09596836211033226>, 2021.

954 Obu, J., Westermann, S., Bartsch, A., Berdnikov, N., Christiansen, H. H., Dashtseren, A., Delaloye, R., Elberling, B.,
955 Etzelmüller, B., Kholodov, A., et al.: Northern Hemisphere permafrost map based on TTOP modelling for 2000–2016 at 1
956 km² scale, *Earth-Science Reviews*, 193, 299–316, <https://doi.org/10.1016/j.earscirev.2019.04.023>, 2019.

957 Painter, S. L. and Karra, S.: Constitutive model for unfrozen water content in subfreezing unsaturated soils, *Vadose Zone*
958 *Journal*, 13, <https://doi.org/10.2136/vzj2013.04.0071>, 2014.

959 Porter, C., Morin, P., Howat, I., Noh, M., Bates, B., Peterman, K., Keeseey, S., Schlenk, M., Gardiner, J., Tomko, K., et al.:
960 ArcticDEM, Harvard Dataverse [data set], V1, <https://doi.org/10.7910/DVN/OHHUKH>, 2018.

961 Renette, C.: Parameter files and code for simulations in "Simulating the effect of subsurface drainage on the thermal regime
962 and ground ice in blocky terrain, Norway" [Data set], Zenodo, <https://doi.org/10.5281/zenodo.6563651>, 2022.

963 Romundset, A., Bondevik, S., and Bennike, O.: Postglacial uplift and relative sea level changes in Finnmark, northern Norway,
964 *Quat. Sci. Rev.*, 30, 2398-2421, <https://doi.org/10.1016/j.quascirev.2011.06.007>, 2011.

965 Sæmundsson, Þ., Morino, C., Helgason, J. K., Conway, S. J., and Pétursson, H. G.: The triggering factors of the Móafellshyrna
966 debris slide in northern Iceland: Intense precipitation, earthquake activity and thawing of mountain permafrost, *Science of the*
967 *total environment*, 621, 1163–1175, <https://doi.org/10.1016/j.scitotenv.2017.10.111>, 2018.

968 Saloranta, T.: Simulating snow maps for Norway: description and statistical evaluation of the seNorge snow model, *The*
969 *Cryosphere*, 6, 1323–1337, <https://doi.org/10.5194/tc-6-1323-2012>, 2012.

970 ~~van~~ [Scudeler, C., Paniconi, C., Pasetto, D., and Putti, M.: Examination of the seepage face boundary condition in subsurface](#)
971 [and coupled surface/subsurface hydrological models, *Water Resources Research*, 53\(3\), 1799-1819, 2017.](#)

972 [Schmidt, J. U., Eitzelmüller, B., Schuler, T. V., Magnin, F., Boike, J., Langer, M., and Westermann, S.: Surface temperatures](#)
973 [and their influence on the permafrost thermal regime in high-Arctic rock walls on Svalbard, *The Cryosphere*, 15, 2491–2509,](#)
974 <https://doi.org/10.5194/tc-15-2491-2021>, 2021.

975 [Smith, M. and Riseborough, D.: Climate and the limits of permafrost: a zonal analysis, *Permafrost and Periglacial Processes*,](#)
976 [13, 1–15, <https://doi.org/10.1002/ppp.410>, 2002.](#)

977 [Van](#) Everdingen, R. O.: Multi-language glossary of permafrost and related ground-ice terms, International Permafrost
978 Association, 1998.

979 Vionnet, V., Brun, E., Morin, S., Boone, A., Faroux, S., Le Moigne, P., Martin, E., and Willemet, J.-M.: The detailed snowpack
980 scheme Crocus and its implementation in SURFEX v7. 2, *Geoscientific Model Development*, 5, 773–791,
981 <https://doi.org/10.5194/gmd-5-773-2012>, 2012.

982 Westermann, S., Schuler, T., Gislås, K., and Eitzelmüller, B.: Transient thermal modeling of permafrost conditions in Southern
983 Norway, *The Cryosphere*, 7, 719–739, <https://doi.org/10.5194/tc-7-719-2013>, 2013.

984 Westermann, S., Langer, M., Boike, J., Heikenfeld, M., Peter, M., Eitzelmüller, B., and Krinner, G.: Simulating the thermal
985 regime and thaw processes of ice-rich permafrost ground with the land-surface model CryoGrid 3, *Geoscientific Model*
986 *Development*, 9, 523–546, <https://doi.org/10.5194/gmd-9-523-2016>, 2016.

987 Westermann, S., Ingeman-Nielsen, T., Scheer, J., Aalstad, K., Aga, J., Chaudhary, N., Eitzelmüller, B., Filhol, S., Kääb, A.,
988 Renette, C., Schmidt, L. S., Schuler, T. V., Zweigel, R. B., Martin, L., Morard, S., Ben-Asher, M., Angelopoulos, M., Boike,
989 J., Groenke, B., Miesner, F., Nitzbon, J., Overduin, P., Stuenzi, S. M., and Langer, M.: The CryoGrid community model

990 (version 1.0) – a multi-physics toolbox for climate-driven simulations in the terrestrial cryosphere, *Geosci. Model Dev.*
991 *Discuss.* [preprint], <https://doi.org/10.5194/gmd-2022-127>, in review, 2022.

992 Wicky, J. and Hauck, C.: Numerical modelling of convective heat transport by air flow in permafrost talus slopes, *The*
993 *Cryosphere*, 11, 1311–1325, <https://doi.org/10.5194/tc-11-1311-2017>, 2017.

994 [Zhang, T.: Influence of the seasonal snow cover on the ground thermal regime: An overview, *Reviews of Geophysics* 43.4,](https://doi.org/10.1029/2004RG000157)
995 <https://doi.org/10.1029/2004RG000157>, 2005.

996 Zweigel, R., Westermann, S., Nitzbon, J., Langer, M., Boike, J., Eitzelmüller, B., and Vikhamar Schuler, T.: Simulating snow
997 redistribution and its effect on ground surface temperature at a high-Arctic site on Svalbard, *Journal of Geophysical Research:*
998 *Earth Surface*, 126, e2020JF005673, <https://doi.org/10.1029/2020JF005673>, 2021.

999